THE GEOLOGICAL SOCIETY OF AMERICA®

A far-traveled basalt lava flow in north-central Oregon, USA

Anthony F. Pivarunas[1,2,†], David R. Sherrod[3], James E. O'Connor[1], Charles M. Cannon[1], and Mark E. Stelten[1,2]

[1]*Geology, Minerals, Energy, and Geophysics Science Center, U.S. Geological Survey, 350 N. Akron Road, Moffett Field, California 94035, USA*

[2]*Volcano Science Center, U.S. Geological Survey, 350 N. Akron Road, Moffett Field, California 94035, USA*

[3]*Volcano Science Center, U.S. Geological Survey, 1300 S.E. Cardinal Court, Vancouver, Washington 98683, USA*

ABSTRACT

Widely separated basalt lava-flow outcrops in north-central Oregon, USA, expose products of a single eruptive episode. A Pliocene lava flow, here informally termed the Tetherow basalt, issued from vents near Redmond, in the Deschutes basin of Oregon, as a plains-forming basalt now exposed in continuous outcrops northward for 60 km. A similar basalt crops out 47 km farther north, near Maupin, within what was then a slightly incised ancestral Deschutes River canyon. The northernmost outcrops of this lava flow lie on Fulton Ridge, in the Dalles basin, near the confluence of the Deschutes and Columbia Rivers. Complementary lines of evidence confirm these rocks are all from the same volcanic eruption. Outcrops in the Deschutes and Dalles basins are chemically similar high-titanium basalts, petrographically similar to each other and distinct from other lava flows in the area. Paleomagnetic directions from 11 scattered sites are similar and indistinguishable by various tests for a common mean. Three new $^{40}Ar/^{39}Ar$ ages indicate the Tetherow basalt eruption occurred between 5.5 Ma and 5.0 Ma, likely at ca. 5.2 Ma. The widely separated outcrops of this lava flow span 160–180 km along the ancestral Deschutes River and downstream Columbia River. The lava flow's length and erupted volume of 15–20 km^3 are extraordinarily large in a non-flood-basalt setting. This lava flow provides a datum with which to describe regional physiographic history, assess incision rates, and infer tectonic history. Spanning different depositional basins, the Tetherow basalt is a useful chronologic and stratigraphic marker bed.

INTRODUCTION

The Cascade volcanic arc is a subduction-related chain of volcanism running along the northwestern United States and southwestern Canada, as oceanic plates descend beneath the North America plate. (Fig. 1, inset; O'Connor et al., 2021a). Detritus shed from the Cascade Range has filled depositional basins behind the arc, such as the Deschutes basin. The Deschutes Formation, representing the late Miocene to early Pliocene infill of the Deschutes basin along the eastern Cascade margin, hosted numerous basaltic eruptions during its depositional period. These lava flows are thought to have generally stayed within their basin of origin (McClaughry et al., 2021a). However, at least one basalt lava flow reached far north to the Dalles basin. This basalt flow creates a new stratigraphic marker that relates the Deschutes and Dalles Formations. Recent mapping and geochemical, geochronological, and paleomagnetic analyses show that the northern outcrops, formerly of unknown source and uncertain age and lying more than 300 m above the modern confluence of the Deschutes and Columbia Rivers in north-central Oregon, USA, correlate to basalt that issued ca. 5.2 Ma from Tetherow Butte, 160 km to the south of the present confluence, and flowed down the ancient Deschutes valley drainage. Here, we report the basis for this correlation, provide new information on the extent, volume, and distribution of this far-traveled lava flow, and interpret the stratigraphic, paleogeographic, and tectonic implications.

GEOLOGIC AND PHYSIOGRAPHIC SETTING

North-central Oregon is underlain by Oligocene and Miocene volcanic and sedimentary strata such as the Eocene–Oligocene Clarno Formation, Oligocene John Day Formation, and flood basalts of the Lower–Middle Miocene Columbia River Basalt Group. The eruptive and erosional late Miocene, Pliocene, and Quaternary deposits originating from the Cascade Range have provided most of the infill in adjacent basins on the east side of the arc in the post–Columbia River Basalt Group landscape (Smith et al., 1987, 1989). The primary regional depocenters of north-central Oregon during late Miocene and early Pliocene time were, south to north, the Deschutes, Tygh Valley, and Dalles basins.

The east flank of the modern Cascade Range in northern Oregon and the three late Miocene to early Pliocene basins are drained by the north-flowing Deschutes River, now incised as much as 600 m below the top of the Columbia River Basalt Group (O'Connor et al., 2003a). The Deschutes River joins the west-flowing Columbia River in Dalles basin, where the Columbia River has incised into post–Columbia River Basalt Group volcaniclastic-fluvial deposits. This study was motivated by ongoing geologic mapping in Dalles basin (Cannon and O'Connor, 2019; O'Connor et al., 2021a), which prompted an investigation for the source of the ridge-top basalt flow mapped by Newcomb (1969) as part of the Dalles Formation. Two new $^{40}Ar/^{39}Ar$ ages of ca. 5.4 Ma and normal-polarity field measurements from Dalles basin outcrops suggested a possible correlation to the Tetherow Butte member of the Deschutes Formation, which has an age of 5.31 ± 0.05 Ma and normal-polarity magnetization (Smith and Hayman, 1987).

Setting of the Tetherow Basalt

Lava from Tetherow Butte flowed through three late Miocene to early Pliocene basins before entering the Columbia River valley

James E. O'Connor https://orcid.org/0000-0002-7928-5883

[†]apivarunas@usgs.gov

GSA Bulletin;
published online 22 January 2024

https://doi.org/10.1130/B37178.1.

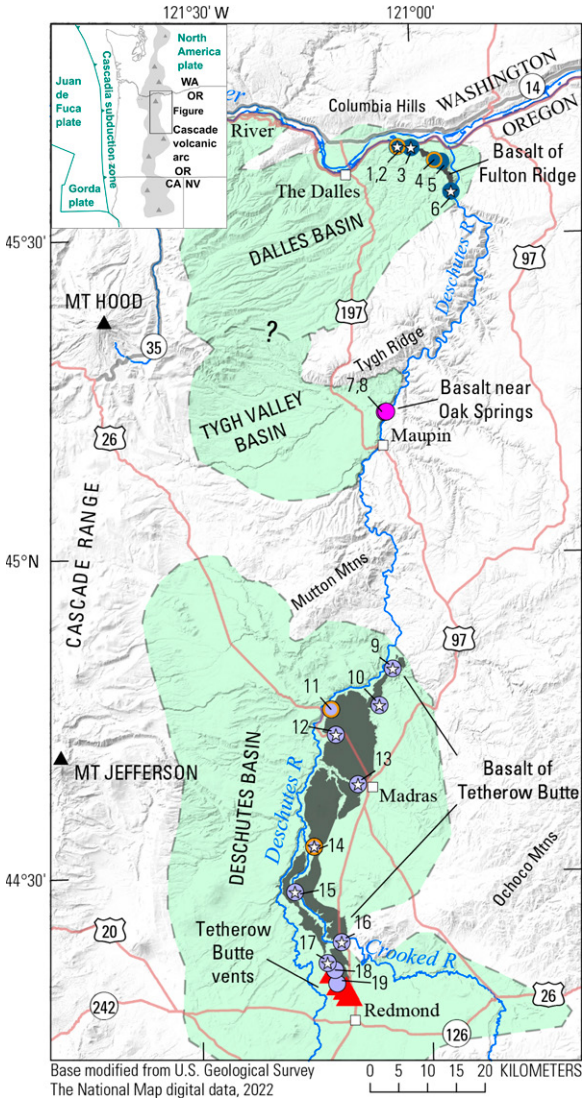

Figure 1. Map of north-central Oregon showing regional flow path of the Tetherow basalt, from vents at Tetherow Butte to Fulton Ridge. Basalt distribution is shaded dark gray. Green shade indicates basins traversed by the Tetherow basalt. Red triangles indicate area of scoria cones inferred to be vents of Tetherow basalt. Filled circles and numerical labels indicate locations of geochemical analyses in Tables 1 and 2; colors of fill correspond with flow location (see geochemical analysis symbols in Figs. 5 and 6). White stars indicate determinations of paleomagnetism in Table 3. Hollow orange circles indicate locations of $^{40}Ar/^{39}Ar$ age determinations in Table 4. Inset shows general geographic location of Figure 1 in western North America. WA—Washington; OR—Oregon; CA—California; NV—Nevada; R—river.

(Fig. 1). For simplicity, we refer to all products of the eruptions as the informal, unranked Tetherow basalt, previously described as the Tetherow Butte member of the Deschutes Formation (Smith, 1986) and basalt of Fulton Ridge (Newcomb, 1966).

ANALYSIS AND FINDINGS

The field relations and geochronologic, geochemical, and paleomagnetic measurements (data in Pivarunas et al., 2023) described in the following sections indicate that the outcrops in all three late Miocene to early Pliocene basins are part of the same extensive and far-traveled basalt flow that issued from Tetherow Butte.

Field Observations and Relations

We examined and sampled 30 outcrops of this lava flow, from the Deschutes to the Dalles basins as well as the intervening Deschutes River canyon outcrop near Tygh Valley (Fig. 1). Summary data on flow thickness and field relations are presented in Table S1[1] (Pivarunas et al., 2023).

The lava path (lava km) is described as the distance northward, in kilometers, from the contact between the lava flow and the Tetherow basalt's northern vent deposits (Fig. 1). The lava path is drawn as the roughly north-trending midline of the flow's inferred distribution.

Flow Extent and Thickness

Deschutes basin. The Tetherow basalt is thickest and most extensive in the Deschutes basin, where it erupted from four northwesterly aligned source vents flanked by cinder and scoria cones 5 km north-northwest of Redmond, central Oregon (Fig. 2). Namesake Tetherow Butte is ~3 km east of the Deschutes River. The lava and its vent deposits have been assigned to the Tetherow Butte member of the Deschutes Formation (Smith, 1986, p. 161).

Tetherow lava flowed northward from the vent area, attaining as much as 70 m of thickness (Robinson and Stensland, 1979; Smith, 1986, p. 166). The pathway was through a broad valley (~lava km 15; Fig. 2, cross section A–A′; Fig. 3), defined to the east by the highland of Oligocene rocks along the western edge of the Ochoco Mountains and to the west by the east-sloping volcaniclastic apron from the High Cascades. The Tetherow basalt is 4–5 km wide along this reach.

Upon reaching the latitude of Madras (~lava km 40; Fig. 2, cross section B–B′; Fig. 3), the advancing lava spread laterally east and west to 9–10 km wide, forming the underpinnings of what is now termed the Agency Plains, an upland surface today bounded mostly by rimrock cliffs of Tetherow basalt. The preserved thickness of basalt diminishes along the Agency Plains, exceeding 25 m in only a few areas (Table S1).

North beyond Agency Plains, the Tetherow basalt map pattern narrows to 1–2 km wide, suggesting the lava flow was confined by valley slopes. At the Trout Creek confluence with the Deschutes River, just north of the town of Gateway at numbered location 9 on Figure 1 (~lava km 61; Fig. 3, cross section C–C′), the basalt thickens to as much as 40 m, indicating that the Tetherow lava flow entered a constricted intracanyon setting at the south flank of the Mutton Mountains uplift.

Tygh Valley. Down the canyon along the Deschutes River, no outcrops of Tetherow basalt are known between the Trout Creek confluence and Maupin (~lava km 107), a stretch where landslides have broadened the canyon and dragged away potential remnants of Tetherow basalt. North of Maupin, at the east margin of Tygh basin, an outcrop of Tetherow basalt persists on the east canyon wall on a promontory opposite from the Oak Springs fish hatchery, ~220 m above the Deschutes River (~lava km 108; Fig. 3, cross section D–D′). We term this the "basalt near Oak Springs." This sliver of lava is likely the preserved eastern edge of Tetherow basalt in an intracanyon setting.

The Deschutes River canyon north from Oak Springs lacks detailed study. Outcrops of Tetherow basalt may lie undiscovered. If present, they are likely preserved at fortuitous sites ~200 m above the river (Fig. 4) as small promontories or as capping ledges on bedrock exposures of Columbia River Basalt Group lava flows

[1]Supplemental Material. Tables with field, geochemical, and geochronological data. Please visit https://doi.org/10.1130/GSAB.S.24765021 to access the supplemental material, and contact editing@geosociety.org with any questions.

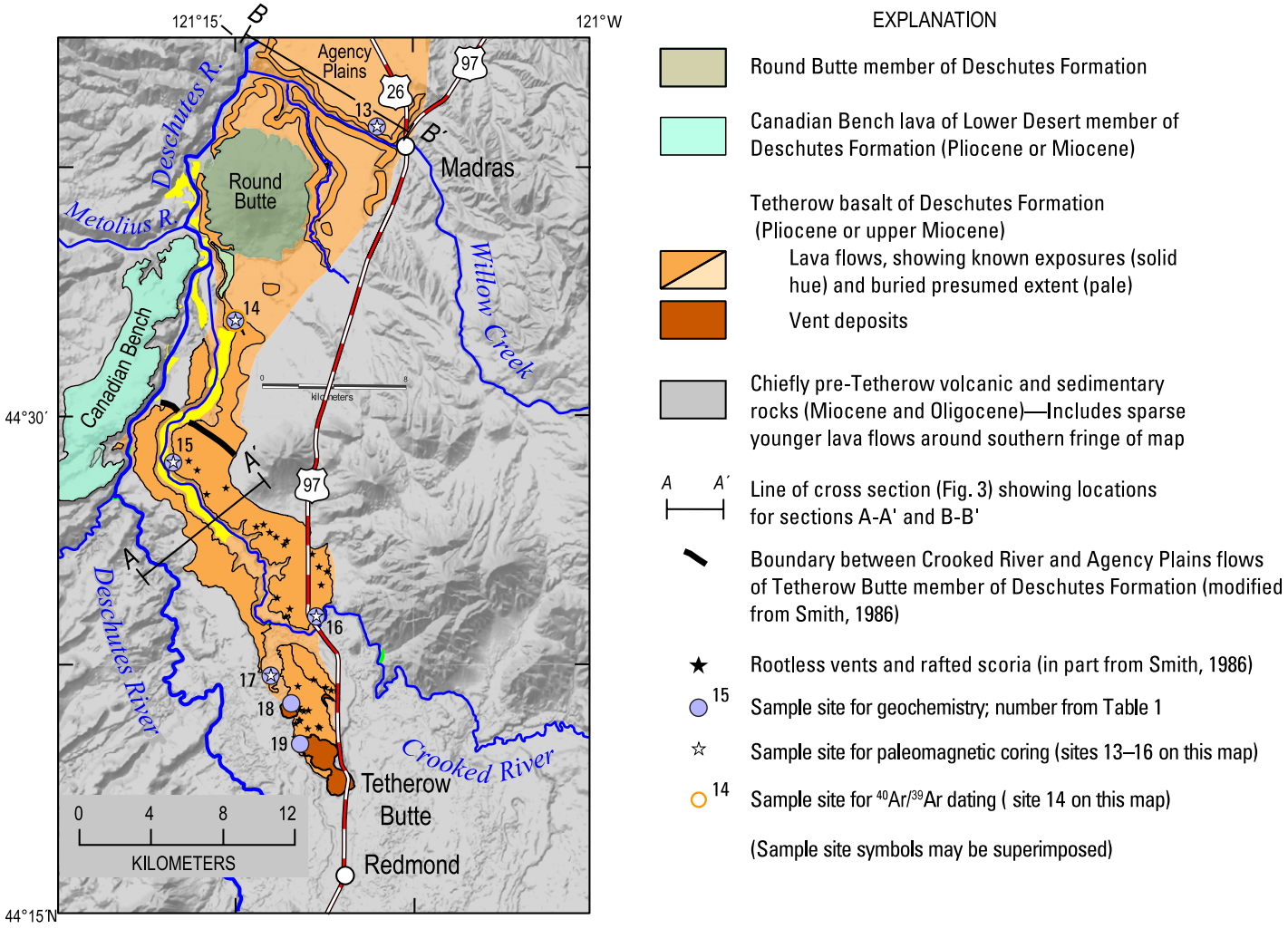

Figure 2. Simplified geologic map of the southern extent of Tetherow basalt. Hillshade base map is from The National Map (U.S. Geological Survey, 2022a). Bold black line indicates boundary between Crooked River (south of line) and Agency Plains (north of line) flows of the Tetherow Butte member of Deschutes Formation (modified from Smith, 1986). The slightly younger Canadian Bench lava and younger Round Butte member of the Deschutes Formation are shown as well. Cross-section lines refer to profiles in Figure 3. R—river.

within more deeply incised oxbows of the modern Deschutes River.

Dalles basin. Within Dalles basin, the Tetherow basalt underlies Fulton Ridge, a northwest- to west-trending landform that begins along the west side of the Deschutes River valley at about Deschutes River mile 5.5, in the area of the historic, abandoned Freebridge crossing (Fig. 5). The ridge is mantled by eolian deposits of Pleistocene age, chiefly loess, which cover the basalt. Northwest and west from Freebridge, Fulton Ridge parallels the Columbia River valley for 10 km (O'Connor et al., 2021a, p. 167). The westernmost known outcrop is on Kaser Ridge, a fault-displaced (Anderson et al., 2013) downvalley continuation of Fulton Ridge (Fig. 5).

The areal extent of these previously mapped (Newcomb, 1966) northern outcrops of Tetherow basalt on Fulton Ridge is ~8 km^2, judging from the lava flow's ridge-top edges. The top of the flow is ~320 m above the predam elevation of the Deschutes and Columbia confluence (~lava km 175; Fig. 3, cross section E–E′). Our thickness measurements ranged between 7 m and 18.2 m (Table S1), which agree with the 17 m (55 ft) reported by Newcomb (1966).

Outcrop Appearance and Setting

In most exposures, the Tetherow basalt crops out with a distinctive morphology consisting of a columnar-jointed lower third; a once-glassy entablature but now intensely spheroidally weathered middle third (e.g., "columnar-spheroidal" weathering as described in Windom et al., 1981); and a columnar or blocky, variably scoriaceous upper third, commonly with a flow top of scoriaceous agglutinate. The weathered middle third commonly erodes recessively, leaving the erosionally resistant lower and upper parts to crop out boldly, as if they represent two separate lava flows (Fig. 6). This outcrop appearance is ubiquitous along rimrock exposures northward from lava kilometer 12 in the central Deschutes basin, as far south as incision has cut through the Tetherow basalt. An accessible outcrop was found at the road cut where SW Canyon Road, the western extension of Avenue C from Madras, ascends through a full exposure of the Tetherow basalt (Fig. 2, site 13; lat and long 44.6420°N, 121.1512°W).

Two exceptions to this typical appearance are outcrops that exhibit a fanning colonnade, the most striking of which is displayed where High-

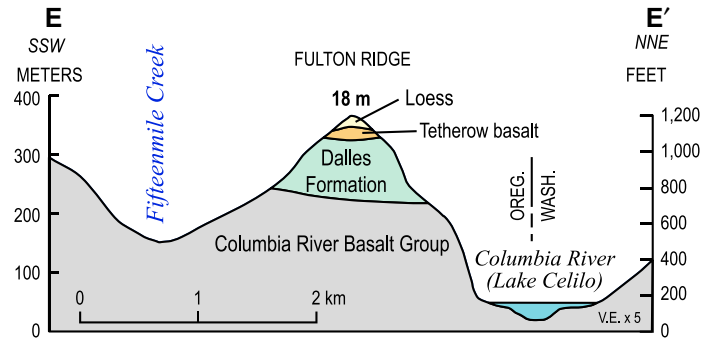

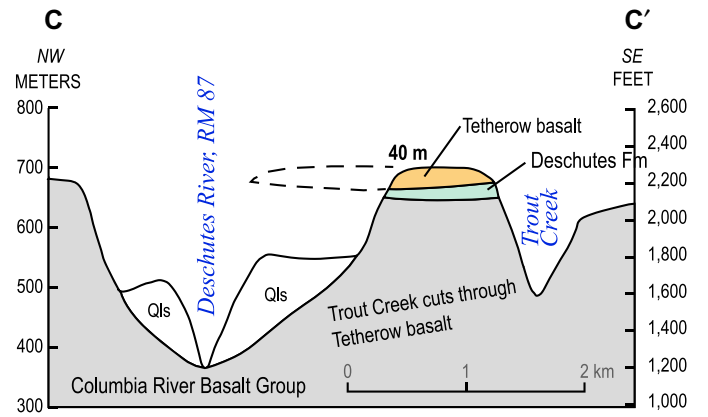

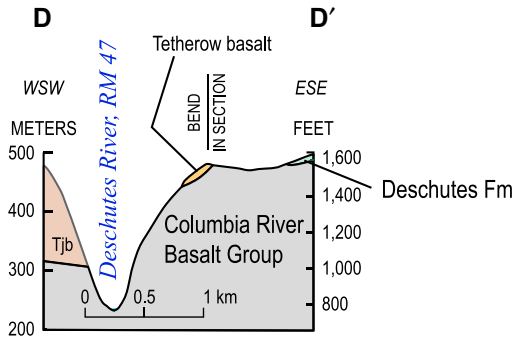

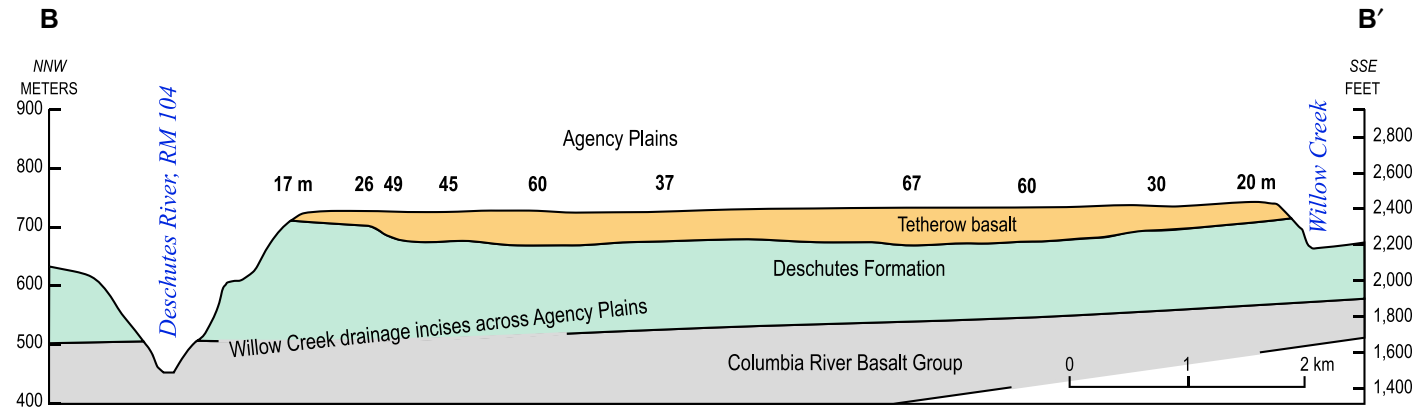

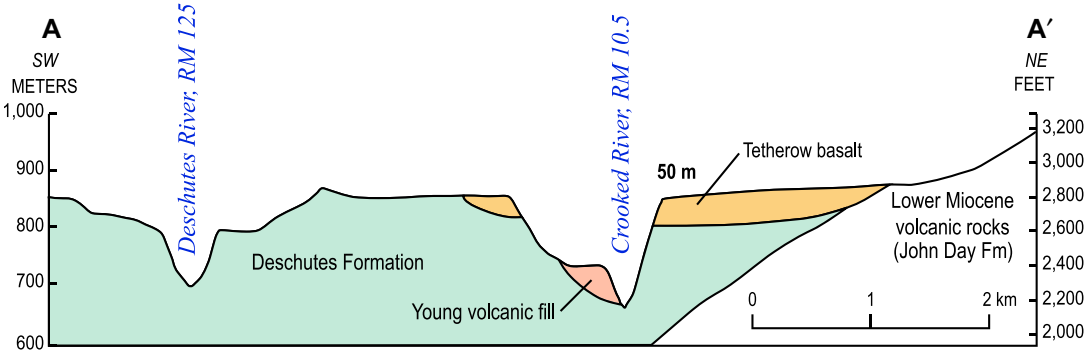

Figure 3. Representative cross-section profiles at five mapped locations, described in text. These sections delineate the general character of the flow at each reach. A–A′ and B–B′ profile line locations are shown in Figure 2. Vertical scale is in feet on right side and meters on left side of profile; elevations are relative to sea level. Note changing vertical range; profiles are scaled similarly with 5× vertical exaggeration (V.E.). Unit symbol Qls in cross section C–C′ indicates Quaternary landslide deposits. Unit symbol Tjb in cross section D–D′ indicates basalt of Juniper Flat, age ca. 3 Ma. Numbers along top of profile are lava thicknesses (in meters). OREG.—Oregon; WASH.—Washington; RM—river mile; Fm—Formation.

way 26 descends northwest off Agency Plains (Table S1). In both instances, the outcrop characteristics and distribution indicate a channel or canyon-fill setting.

Smith (1986) subdivided his Tetherow Butte member of the Deschutes Formation into the Agency Plains basalt flow and the overlying Crooked River basalt flow, suggesting (p. 166) "most places cooled together to form a single thick entablature with thin upper and lower colonnades." The Agency Plains basalt flow as mapped by Smith (1986, 1987a, 1987b) and Smith and Hayman (1987) extends 60 km north, to near river mile 86 of the Deschutes River, underlying the vast 250 km^2 Agency Plains north and west of Madras. At its north limit, it partly fills a 1-km-wide paleovalley incised into Columbia River Basalt Group at the north extent of the Deschutes Formation. The Crooked River basalt flow as mapped by Robinson and Stensland (1979) or Smith (1986, p. 166) is much less extensive, and its northern limit is placed near Deschutes River river mile 120 (Fig. 2).

The outcrop pattern established by the heavily weathered middle third of the Tetherow basalt has probably contributed to previous interpretations of two separate lava flows in the Tetherow basalt. We found it difficult to distinguish or separate the Agency Plains from Crooked River flows by field observations, geochemical analysis, or paleomagnetic directions. The reported observation of a bounding contact describes a discontinuous break in cooling-joint pattern seen in a cliffy bluff on the east bank of the Crooked River (Smith, 1986, p. 164), or occasional flow

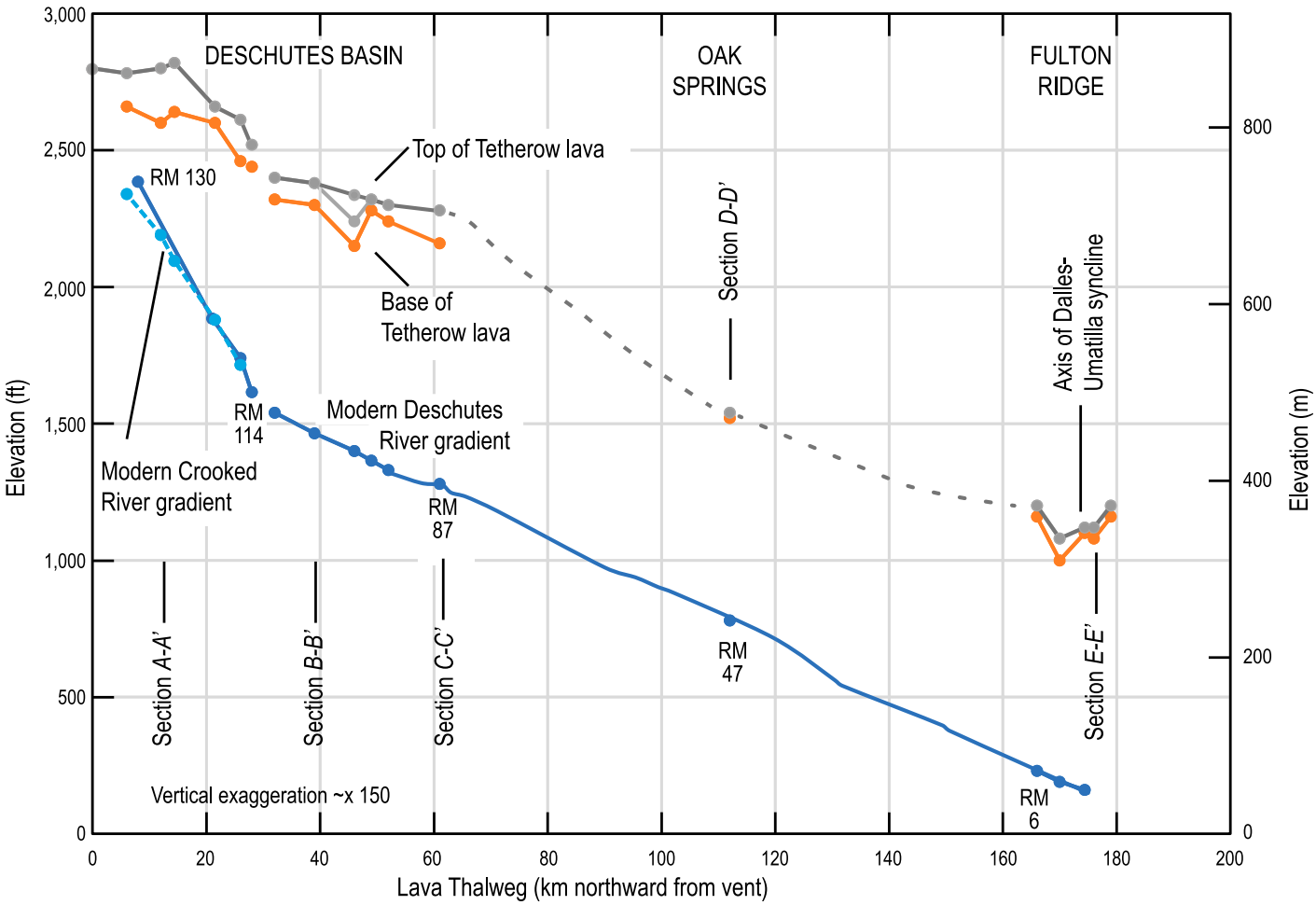

Figure 4. Gradient of Tetherow basalt for its path along the ancestral Deschutes River as defined by elevations at base and top, relative to sea level. Also shown are gradients of modern Deschutes and Crooked Rivers. Lava thalweg is approximate midline of polygon that encloses the extent of known outcrops. North of thalweg km 60, thalweg is approximated by the midline of the canyon occupied by the lava. RM—river mile along Deschutes River, shown for reference, from topographic quadrangle maps. Locations of cross-section profiles for Figure 3 are shown. Tetherow basalt was never present in Deschutes canyon south of river mile 114, so lava elevation measurements are from Crooked River exposures from there south to the vent. Axis of Dalles-Umatilla syncline is from Newcomb (1967, 1969).

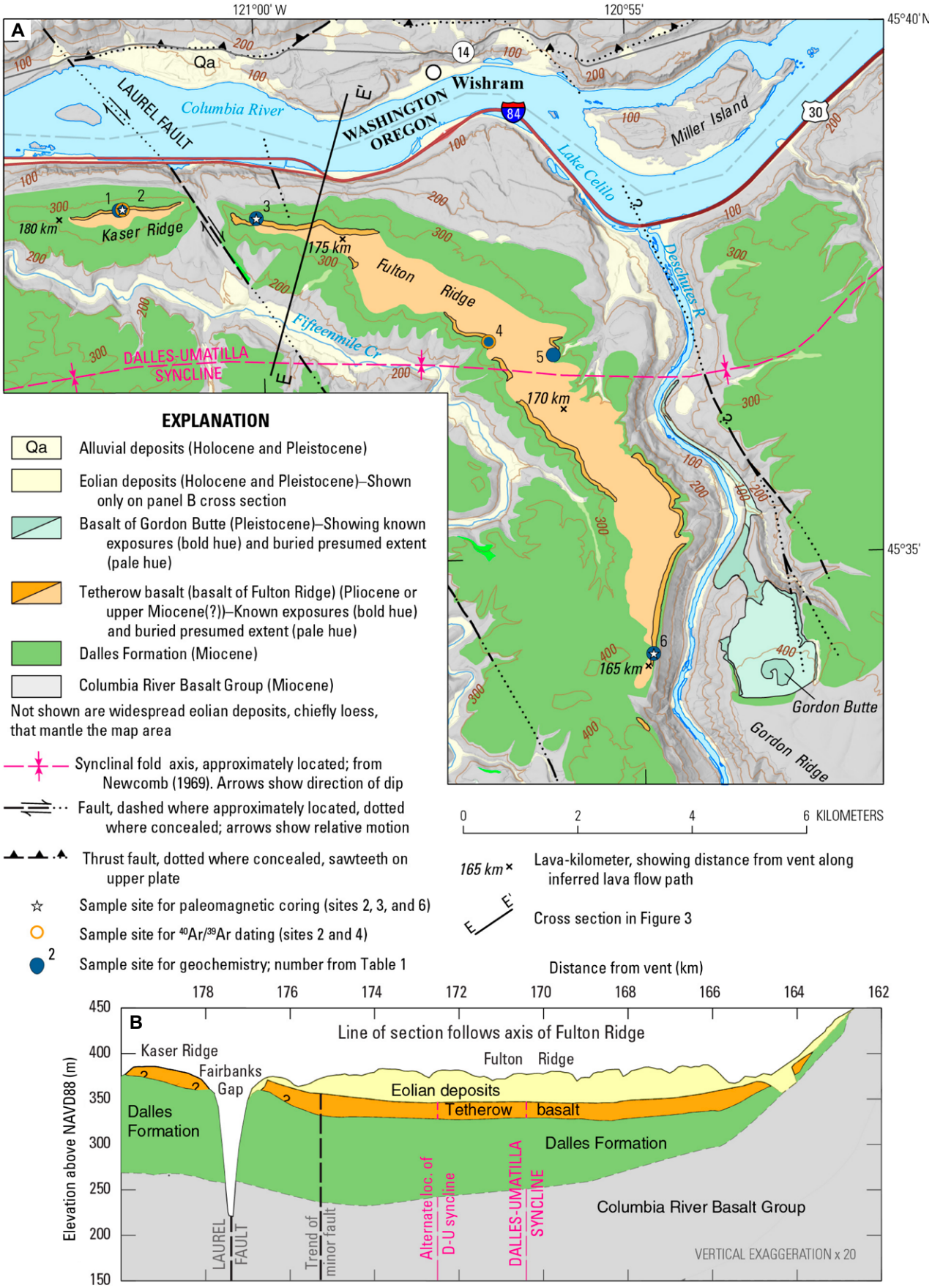

Figure 5. (A) Simplified geologic map of Fulton Ridge area, where the Tetherow basalt was mapped previously as basalt of Fulton Ridge by Newcomb (1966). Hillshade base map is from The National Map (U.S. Geological Survey, 2022b). Thick eolian deposits of Pleistocene age, chiefly loess, mantle much of the area. (B) Cross section drawn along the curvilinear trace of Fulton Ridge; vertical exaggeration is 20×. Values on horizontal axis are lava-kilometer distances from Tetherow vent, as shown on panel A for reference. Deformation across the Dalles-Umatilla (D-U) syncline in the Fulton Ridge area is thought to have begun before emplacement of the Tetherow basalt and continued thereafter, as discussed in text. NAVD 88—North American Vertical Datum of 1988.

breccia (Smith, 1986, p. 166). Our inspection of this break (Fig. 7) did not find convincing evidence of a time break, such as between-flow rubble, a chilled top on the lower flow, sedimentary debris, or a baked horizon; instead, it coincides with the boundary between lower columnar section and the slightly altered middle part of the flow. As an example, take the right side of Figure 6—where the upper blocky section of lava meets the weathered middle—and compare it with the Figure 7C inset, which illustrates the transitions between the upper, middle, and lower parts of the lava flow. We conclude that the Tetherow basalt at the Crooked River Ranch exposure is a single lava-emplacement unit.

Within Deschutes basin, the Tetherow basalt nearly everywhere overlies ignimbrite, fallout tephra, other basalt, and basaltic andesite lava flows, and volcaniclastic fluvial deposits of the Deschutes Formation (Smith, 1986, 1987a, 1987b; Smith and Hayman, 1987; Sherrod et al., 2004). Where preserved as extensive upland benches, like the extensive Agency Plains area, the Tetherow basalt was overlain by as much as 50 m of sediment, which has now largely been removed by erosion except where preserved by overlying lava (Smith, 1986, p. 165). Younger Pliocene lava flows locally overlie the Tetherow basalt in Deschutes basin, such as the Round Butte member (4.0 ± 0.1 Ma, recalibrated age) of the Deschutes Formation (Smith, 1986; Smith et al., 1987; Pitcher et al., 2017).

In its lone Tygh Valley outcrop, the Tetherow basalt lies atop Columbia River Basalt Group lava (Grande Ronde Basalt) and was previously mapped as part of the Columbia River Basalt Group (Waters, 1968; Swanson et al., 1981; Sherrod and Scott, 1995). However, the basalt is inset into the Columbia River Basalt Group. Here, the latter is locally overlain upslope to the southeast by fluvial volcaniclastic gravel characteristic of deposits in the Deschutes Formation (Waters, 1968). Those deposits must predate the Tetherow basalt, given their somewhat higher elevation, marking a time before the ancestral Deschutes River had incised to the Tetherow emplacement elevation.

Within Dalles basin (Fig. 5), the Tetherow basalt commonly shows the outcrop pattern formed by the erosionally resistant flow top and bottom (Fig. 6). One full vertical exposure shows the intensely spheroidally weathered middle section without evidence of discontinuities such as flow breccia, soil, or vesicular zones that would indicate more than one flow. The flow is everywhere capped by sandy and silty loess (Figs. 3 and 5). The flow sits with slight discordance atop the Columbia River Basalt Group at its southernmost exposure along Fulton Ridge (basalt of Fulton Ridge in Newcomb, 1966). Elsewhere it overlies fluvial sandstone and conglomerate or volcaniclastic diamict (inferred as lahar deposits) mapped as Dalles Formation (Newcomb, 1969). In contrast to Newcomb (1969), we found no volcaniclastic strata typical of the Dalles Formation anywhere above the Tetherow basalt in the Fulton Ridge area.

Field Sample Description

Hand specimens were typically dense and medium to dark gray with a fine-grained groundmass containing clear plagioclase phenocrysts up to 3 mm, typically as acicular crystals but occasionally as blocky glomerocrysts, and sparse 0.5 mm yellow-green clinopyroxene; the clinopyroxene phenocrysts were as long as 2 mm. The Tetherow basalt rarely contains visible olivine phenocrysts, unlike other basaltic lava flows of the Deschutes Formation or younger basaltic lava flows from the Newberry area that have entered the Deschutes River canyon.

Geochemistry

Analytical Methods

Samples from 19 localities (Figs. 1, 2, and 3) were analyzed for whole-rock geochemistry. We targeted geochemical sites in the massive lower part of the flow with concessions for outcrop accessibility. Samples were collected and trimmed in the field to avoid weathered and vesicular zones and then further inspected, trimmed, and cleaned before submitting the samples for analysis.

Major- and trace-element concentrations for samples from 16 sites were determined by X-ray fluorescence at Hamilton Analytical Lab (Hamilton College, Clinton, New York) using a Thermo ARL Perform'X spectrometer (see Table 1 for

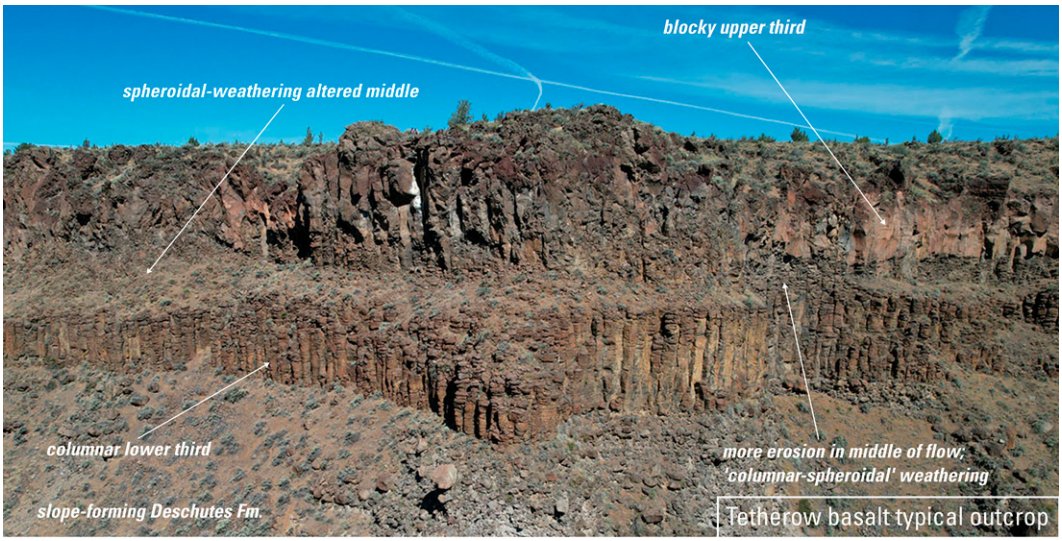

Figure 6. Typical Tetherow basalt rimrock exposure at Cove Palisades State Park. Labels indicate the lower columnar base, recessive-weathering middle, and blocky top with scoriaceous upper section. Drone photograph is by N. Whitley in June 2021, used with permission. Lava outcrop is approximately 46 m high.

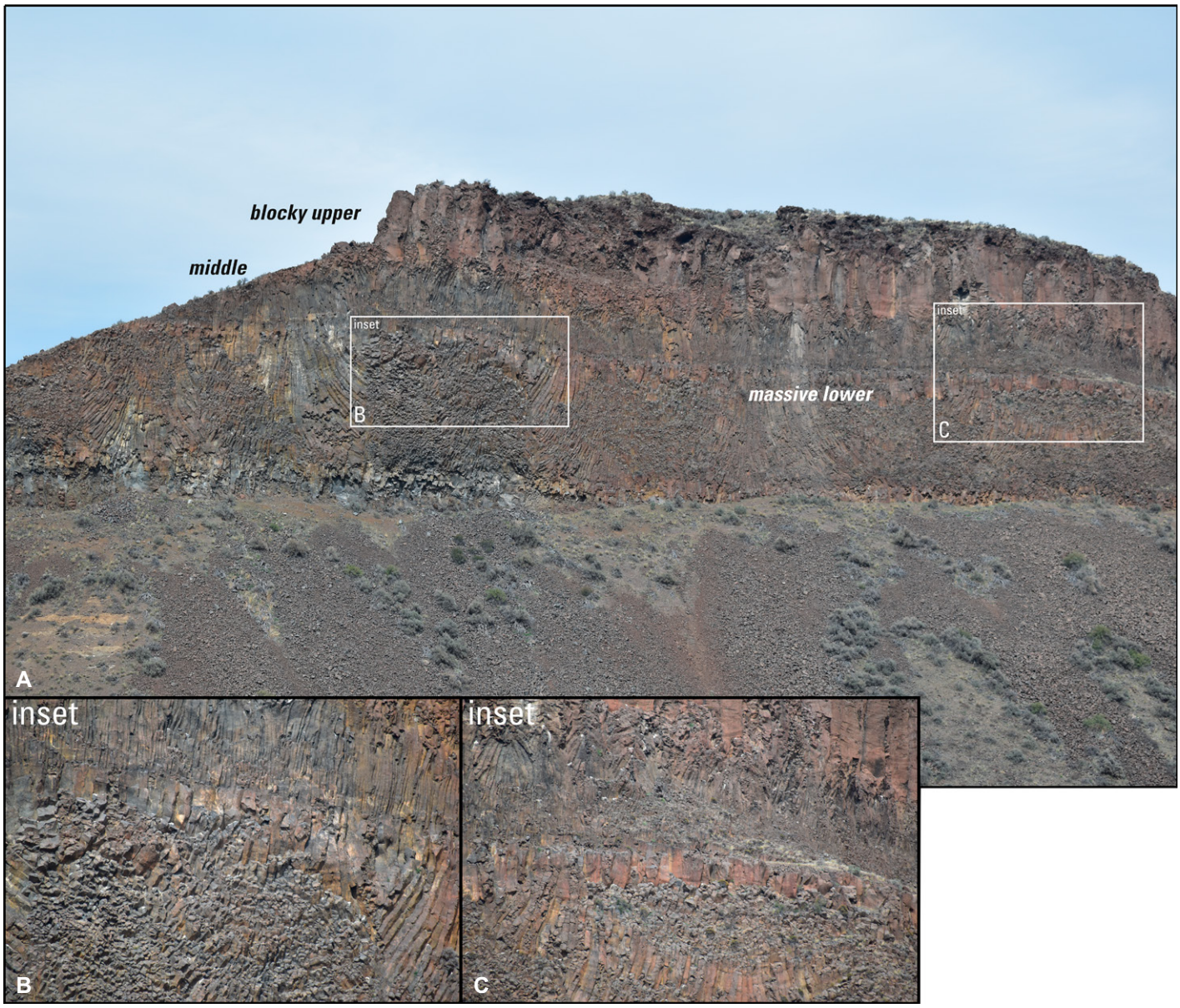

Figure 7. (A) Modern reoccupation of photograph site of Smith (1986, fig. 6.23) showing "break" on east side of Crooked River at Crooked River Ranch. Modern photograph is by D.R. Sherrod in 2022 (U.S. Geological Survey). The break was once interpreted to indicate the presence of two lava flows. (B) Zoomed inset of transition zone between lower columnar section to middle altered section, similar to that seen across the breadth of Figure 6. (C) Zoomed inset of transition zone between altered middle section and upper blocky to crudely columnar-jointed lava, similar to that seen at right side of Figure 6. Lava outcrop is approximately 45 m high.

major-element geochemistry; Table S2 includes trace-element geochemistry; see also Pivarunas et al., 2023). Samples from five sites were analyzed at AGAT laboratory (Calgary, Alberta, Canada), under contract to the U.S. Geological Survey, using X-ray fluorescence for major elements and sodium peroxide fusion inductively coupled plasma–optical emission and inductively coupled plasma–mass spectroscopy to determine trace elements (see Table 1 for major-element geochemistry; Table S3 includes trace-element geochemistry; see also Pivarunas et al., 2023). Two samples (from sites 3 and 14) were split and analyzed by both laboratories to assess interlaboratory variation.

Findings

All samples were from a medium-potassium, high-iron tholeiitic basalt (Fig. 8). They were distinguished by higher concentrations of iron, titanium, and vanadium and lower concentrations of nickel and chromium than other mafic lavas within the Deschutes Formation (Conrey et al., 2004; McClaughry et al., 2021b) and other mafic lavas in the region (Fig. 9). The high Fe content was much more like that of flood basalts of the Columbia River Basalt Group.

Discriminant diagrams for silica versus total alkalis and Ti versus V and Zr, as well as various binary plots, were used to assess the geochemistry of the outcrops of the Tetherow basalt in Deschutes basin, the outcrop near Tygh Valley, and outcrops in Dalles basin. The geochemical

TABLE 1. MAJOR-ELEMENT GEOCHEMISTRY OF TETHEROW BASALT, NORTH-CENTRAL OREGON

Site on map:	1	2	3	3*	4*	5*	6	7	8	9	10	11	12*	13	14	14*	15	16	17	18	18	19
Field sample ID:	JEO_09-24-2014-08(1)	JEO 10-15-2020-1(1)	JEO_06-15-2016-04(1)	JEO_06-15-2016-04(1)	04.26.2016.08	06.14.2016.18(1)	JEO 10-15-2020-2(1)	S20-M2159	S20-M2160	S21-M2321	JEO 10-14-2020-2(1)	S21-M2302	CMC 2018 1006	JEO 10-13-2020-7(1)	JEO 10-13-2020-5(2)	10-13-2020-05	S21-M2319	JEO 10-13-2020-4(1)	S21-M2318	JEO 10-13-2020-2(1)	JEO 10-13-2020-2(2)	JEO 10-13-2020-1(1)
Latitude (°N):	45.639	45.639	45.637	45.637	45.617	45.615	45.567	45.224	45.225	44.822	44.765	44.760	44.720	44.642	44.545	44.545	44.474	44.394	44.362	44.351	44.351	44.330
Longitude (°W):	121.031	121.030	121.000	121.000	120.949	120.935	120.914	121.073	121.069	121.068	121.100	121.206	121.197	121.151	121.249	121.249	121.293	121.194	121.225	121.210	121.210	121.206
SiO_2	51.05	50.62	50.97	51.43	51.50	50.84	51.22	51.28	51.04	51.17	51.00	51.00	50.82	50.99	50.96	50.85	51.22	51.09	51.17	50.75	51.17	50.80
TiO_2	2.42	2.50	2.45	2.50	2.49	2.49	2.37	2.42	2.46	2.44	2.51	2.43	2.52	2.41	2.60	2.61	2.52	2.52	2.50	2.48	2.41	2.48
Al_2O_3	14.41	14.88	14.47	14.55	14.50	14.61	14.36	14.32	14.33	14.38	14.22	14.25	14.11	14.33	14.08	14.06	14.18	14.17	14.25	14.47	14.35	14.22
FeOt	13.44	13.62	13.52	13.46	13.41	13.42	13.32	13.19	13.26	13.32	13.40	13.61	13.62	13.49	13.72	13.62	13.62	13.56	13.49	13.60	13.32	13.59
MnO	0.21	0.20	0.23	0.25	0.22	0.23	0.22	0.23	0.23	0.23	0.24	0.23	0.26	0.22	0.24	0.24	0.24	0.24	0.24	0.24	0.23	0.24
MgO	4.44	4.30	4.57	4.36	4.41	4.79	4.63	4.52	4.69	4.54	4.63	4.63	4.89	4.69	4.56	4.61	4.41	4.48	4.47	4.35	4.63	4.65
CaO	9.17	9.08	8.99	8.81	8.39	8.98	8.92	8.96	8.96	8.88	8.86	8.88	9.05	8.95	8.72	8.89	8.58	8.81	8.77	9.09	8.88	8.89
Na_2O	3.77	3.74	3.68	3.52	3.81	3.54	3.63	3.64	3.68	3.82	3.74	3.73	3.46	3.76	3.67	3.70	3.90	3.77	3.82	3.82	3.79	3.89
K_2O	0.59	0.50	0.60	0.60	0.70	0.56	0.81	0.90	0.80	0.67	0.81	0.69	0.74	0.67	0.84	0.81	0.71	0.73	0.70	0.59	0.70	0.67
P_2O_5	0.51	0.55	0.51	0.51	0.56	0.54	0.53	0.54	0.55	0.56	0.58	0.54	0.54	0.49	0.61	0.61	0.62	0.63	0.59	0.60	0.54	0.57
Totals	100.00	100.00	100.00	100.00	100.00	100.00	100.00	100.00	100.00	100.00	100.00	100.00	100.00	100.00	100.00	100.00	100.00	100.00	100.00	100.00	100.00	100.00
Pre-normalization totals	98.47	98.02	98.20	97.61	98.64	98.55	99.01	99.30	99.67	98.92	99.63	99.49	97.79	99.33	99.71	98.69	99.73	99.19	99.66	99.01	100.10	100.00
LOI	0.51	1.04	0.57	0.51	0.64	0.77	0.09	0.12	−0.30	0.13	−0.32	−0.19	0.48	−0.08	−0.07	0.02	−0.37	−0.04	−0.02	0.16	−0.44	−0.66

Note: Major- and trace-element geochemistry was determined using X-ray fluorescence at Hamilton Analytical Lab (Hamilton College, Clinton, New York, USA) on a Thermo ARL Perform'X spectrometer. Site numbers are keyed to the map depicted in Figure 1. Major-element concentrations are expressed as oxides in weight percent. Trace elements are expressed in parts per million. Major-element concentrations were normalized to 100%, volatile free, with pre-normalization totals provided. FeOt—total iron as FeO; LOI—loss on ignition. Additional geochemical data are available in Pivarunas et al. (2023). For full latitude and longitude precision, see Tables S2 and S3 (text footnote 1).

*Major- and trace-element geochemistry analyzed at AGAT Laboratories (Calgary, Alberta, Canada), under contract to the U.S. Geological Survey.

similarity among these samples (Fig. 8) and their difference from other lavas in the region (Fig. 9) strongly suggest that all analyses were indeed from the same flow. The Ti versus V ratios for Tetherow basalt samples showed the greatest similarity to the Grande Ronde Basalt of the Columbia River Basalt Group (Fig. 9). In addition, we calculated the quantitative similarity coefficient of Borchardt et al. (1972), which was in all cases above 0.91 (Table 2). The samples split and analyzed at separate laboratories had even higher similarity coefficients of 0.98 for sample 3 and 0.99 for sample 14. This suggests no analytically detectable differences between analyses at the different laboratories.

Paleomagnetism

Analytical Methods

Samples were collected and processed from 11 sites (Fig. 1) using standard paleomagnetic sampling protocols (Butler, 1992). At each site, 8–14 cores as long as 12 cm were drilled with a gasoline-powered, water-cooled, diamond-bit coring drill. Samples were oriented in the field using a Pomeroy orienting device with a magnetic compass; a built-in sun compass was also used for orientation when possible. Orientations from sun compass measurements were preferred; magnetic compass directions were corrected using either average site declination from sun compass measurements or International Geomagnetic Reference Field (IGRF) declination at the site location. Sites T201 through T204 and T211 through T214 were taken from the Tetherow Butte member of the Deschutes Formation (Smith, 1986) in Deschutes basin. Sites T205, T206, and T221 were obtained from basalt outcrops near the confluence of the Deschutes River with the Columbia River in Dalles basin.

Specimens were analyzed in the U.S. Geological Survey Paleomagnetics Laboratory in Menlo Park, California, using a cryogenic magnetometer (2G DC-SQUID) with an automated sample-handling (RAPID) system, contained in a magnetically shielded room. A specimen from each sample was demagnetized using stepwise alternating fields from in-line coils above the magnetometer; selected twin specimens were demagnetized using thermal methods. Curie temperatures were measured in air on powdered specimen material using a susceptibility meter with a furnace attachment.

Findings

Field-measured fluxgate magnetometer readings showed that outcrops in all three basins carry normal paleomagnetic directions (Sherrod et al., 2004; J.L. Anderson, UH-Hilo, 2020, oral commun.). Magnetic remanence is carried by

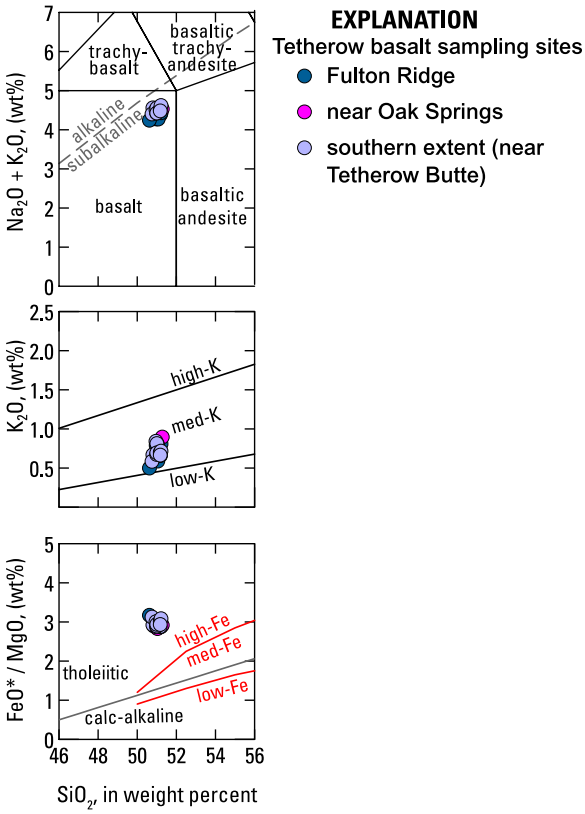

Figure 8. (A) International Union of Geological Sciences classification (Le Maitre, 2002) showing alkaline-subalkaline discriminant of Irvine and Baragar (1971) as dashed line. (B) High-, medium-, and low-K_2O fields extended from Gill (1981). (C) Classification as tholeiitic versus calc-alkaline according to Miyashiro (1974) with high-, medium-, and low-iron (Fe) fields of Arculus (2003).

titanomagnetite, as determined from susceptibility-temperature experiments (Fig. 10). We noted two types of behavior in these experiments, described here as types A and B. The susceptibility-temperature curve type A, seen in four sites, showed a moderate rise in susceptibility before a sharp drop at low-titanium titanomagnetite blocking temperatures (Fig. 10A). This was followed by a similar-shaped but lower-susceptibility cooling curve. In five sites, type B behavior was noted, in which a rapid rise and an equally rapid drop in susceptibility took place from room temperature to ~120 °C, followed by a slight rise to ~580 °C and then another drop (Fig. 10B). Cooling curves for these sites showed a substantial susceptibility increase as the samples cooled through magnetite blocking temperatures. This suggests a high-titanium titanomagnetite as the major remanence carrier at these sites (Dunlop and Özdemir, 2001; Tauxe, 2010), consistent with rapid quenching in these areas of the lava flow. Upon heating, the magnetic susceptibility was then dominated by newly formed low-titanium titanomagnetite. Two sites, T204 and T211, exhibited elements of both behaviors. Both sites with "mixed" behavior were in thinner (~9 m thick) sections of the lava flow. The differences in magnetic mineralogy, however, did not substantially affect the directional data.

Typical secondary directional components were low-coercivity viscous magnetizations and randomly directed magnetizations of medium to high coercivity (Fig. 11). These more persistent components were probably isothermal remanent magnetizations from nearby lightning strikes (Cox, 1961); sampling was spread around outcrops to mitigate this effect. Characteristic remanent magnetic directions for specimens were calculated using principal component analysis (Kirschvink, 1980) on data in vector-component diagrams, which were then averaged at the site level using conventional Fisher (1953) statistics. Specimens with a large secondary component that failed to reach a stable end point were instead fit with great-circle planes (Fig. 11).

After demagnetization, all sites showed north to slightly east of north, moderate-down inclination components (Table 3; Fig. 12A; see also https://doi:10.7288/V4/MAGIC/19605). Paleomagnetic directions from eight southerly sites in Deschutes basin had a slightly east of north declination (D) and moderate inclination (I). The mean direction obtained from averaging all these sites ($N = 8$) was $D = 5.0°$, $I = +54.6°$ ($\alpha_{95} = 2.6°$, $\kappa = 440$). Individual site-mean directions nearly all overlapped at 95% confidence. Three sites with relatively low inclinations (+50.0° to +51.8°) formed a particularly tight cluster within the overall group. The three northerly Dalles basin sites also shared a common direction of magnetization and gave a mean ($N = 3$) of $D = 4.4°$ and $I = +59.2°$ ($\alpha_{95} = 5.2°$, $\kappa = 557$).

We accounted for the ~1° of latitude separating the eight Deschutes basin sites (representative latitude 44.5°N) from the three Dalles basin sites (representative latitude 45.5°N) by converting the north direction to a virtual geomagnetic pole and then calculating the equivalent paleomagnetic direction expected at the mean latitude of the southerly sites (~44.5°N) by ~1° of latitude. We used this adjusted value for the northern sites for all comparisons (Fig. 12B). The difference in mean paleomagnetic directions between the Deschutes basin samples and those from Dalles basin was 3.7°.

Multiple statistical tests suggested that the site-mean directions are likely (95%) from a distribution that shares a common mean, and that the null hypothesis—stating that the two mean directions are the same—cannot be rejected (at 95% confidence) (Watson, 1956; McFadden and Lowes, 1981; McFadden and McElhinny, 1990). The probabilistic algorithm of Bogue and Coe (1981) suggested that the mean directions have a 0.74 probability of being "simultaneous"; i.e., there was little movement of the geomagnetic field while magnetic remanence was set for the basalt outcrops in both the Deschutes and Dalles basins. This result contrasts with just a 0.06 probability that the similar magnetic orientations are due to the fortuitous recurrence of directions ("random"). A Bayesian recasting of the MM1990 reversals test (Heslop and Roberts, 2018) also provided strong positive support (probability 0.94) for a common mean paleomagnetic direction between south and north samples. This battery of statistical tests indicated that the Deschutes basin and Dalles basin lavas had their paleomagnetic directions set simultaneously, at least to the 3°–5° resolving power of paleomagnetism due to experimental effects, local magnetic anomalies, and outcrop-level deformation (Doell and Cox, 1963; Holcomb et al., 1986; Hagstrum and Champion, 1994; Böhnel and Schnepp, 1999). Considering all 11 sites as the same flow, the mean direction for the Tetherow basalt is $D = 4.4°$, $I = +55.2°$ ($\alpha_{95} = 2.3°$, $\kappa = 384$). This direction does not average secular variation; its virtual geomagnetic pole is at 80.4°N, 37.1°E ($A_{95} = 2.6°$, K = 312).

$^{40}Ar/^{39}Ar$ Geochronology

Analytical Methods

We collected three samples from the Tetherow basalt for $^{40}Ar/^{39}Ar$ dating (Table 4; see Table S4 for data; Pivarunas et al., 2023). Two samples, JEO-9-24-14-08 and JEO-12-21-17-03,

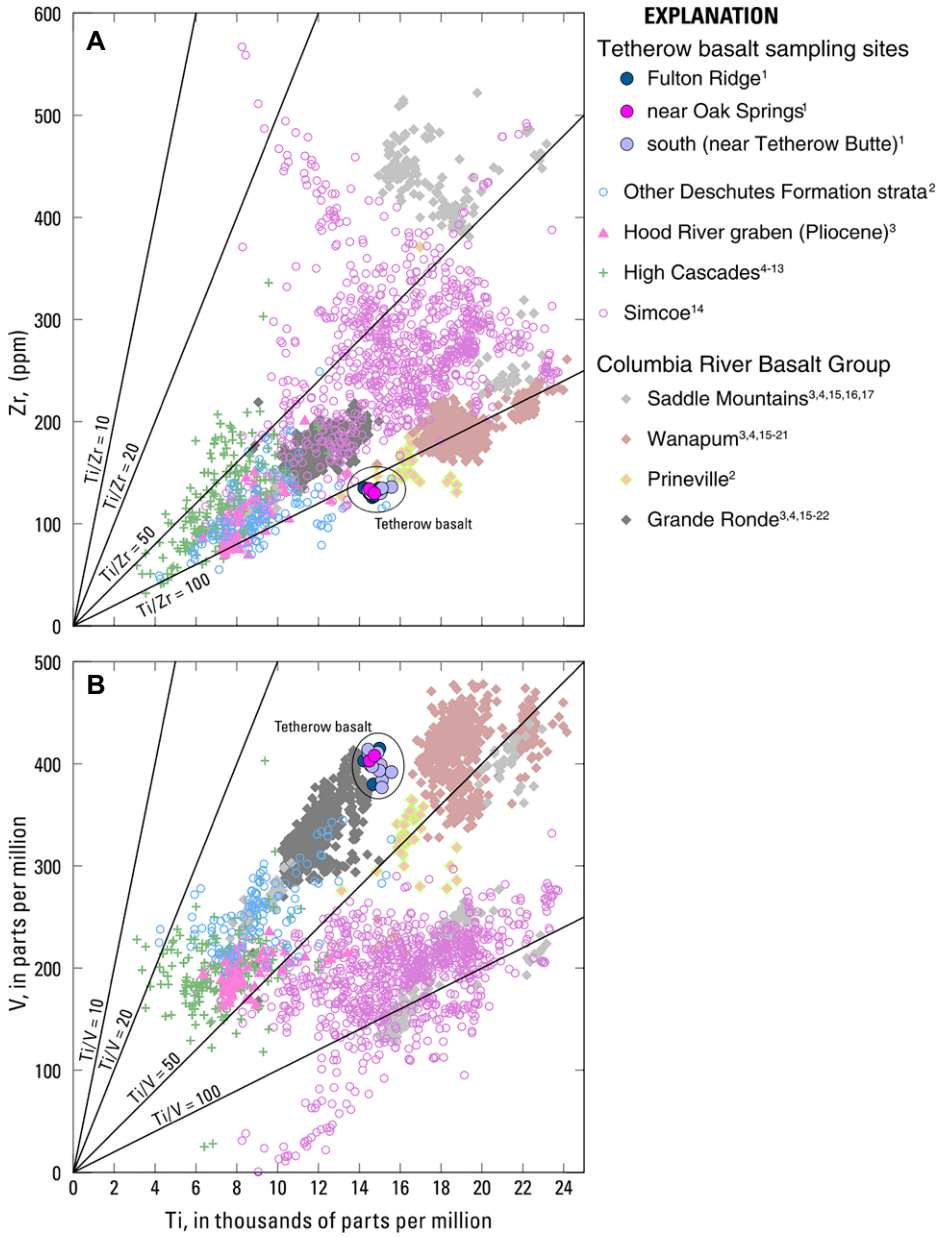

Figure 9. Geochemical variation of (A) zirconium and (B) vanadium (after Shervais, 1982) versus titanium for representative Neogene basaltic lava flows of the eastern Columbia Gorge, Deschutes River basin, and Dalles-Umatilla syncline of Newcomb (1967). Titanium was computed from recalculated analyses with major elements expressed as oxides and total iron as FeO and values normalized to 100% on a volatile-free basis. Samples from Hood River graben are those of Pliocene map units of McClaughry et al. (2012). Samples from the Simcoe Mountains volcanic field are from the area of Yakama Reservation (Hildreth and Fierstein, 2015). For Columbia River Basalt Group lava (CRBG), samples of Saddle Mountains, Wanapum, and Grande Ronde basalts are limited to members known to have reached the southern Columbia Plateau. Data sources are indicated by superscripts in unit groupings: 1—this study; 2—McClaughry et al. (2021a); 3—McClaughry et al. (2012); 4—GEOROC/DIGIS Team (2020); 5—Bacon et al. (1997); 6—Conrey et al. (1997); 7—Conrey et al. (2001); 8—Hughes (1990); 9—Leeman et al. (2005); 10—Rowe et al. (2009); 11—Schmidt and Grunder (2009); 12—Schmidt and Grunder (2011); 13—Carlson et al. (2018); 14—Hildreth and Fierstein (2015); 15—Bowman et al. (2015); 16—Oregon Water Resources Department (2020); 17—Yuh et al. (2022); 18—Madin and McClaughry (2019); 19—McClaughry et al. (2021b); 20—McClaughry et al. (2020); 21—Woodring (2020); 22—Sawlan (2018).

were taken from the northern basalt outcrops in Dalles basin; the former, JEO-9-24-14-08, was collected at paleomagnetic site T205. A third sample, JEO-10-13-2020-5(1), was taken from Deschutes basin in a roadside quarry coincident with paleomagnetic site T202—the same outcrop that produced the $^{40}Ar/^{39}Ar$ age reported by Smith et al. (1987). Field collection entailed hammer-trimming >1 kg of dense, unweathered sample. The samples were further trimmed and cleaned in the office to remove any remaining weathered or otherwise altered material. From the resulting material, a chip was retained for preparation of a thin section, and the remainder was processed for dating.

The three new samples dated for this study were crushed, ultrasonicated, and sieved for grain size 250–355 μm. Groundmass was separated as much as possible from phenocryst phases using a Frantz magnetic separator and handpicking under a binocular microscope. (Note: Broken phenocrysts may end up in "groundmass" separates; this is true for all mineral separations. Although one can handpick and magnetically separate out most of the intact phenocrysts, small broken phenocryst pieces are not easy to separate.)

Approximately 100 g aliquots of material were prepared for each groundmass separate. The separates were packaged in Al foil along with Bodie Hills sanidine monitor minerals (9.7946 ± 0.0031 Ma; Fleck et al., 2019) and encapsulated in quartz vials. The quartz vials were wrapped in 0.5-mm-thick Cd foil to shield samples from thermal neutrons during irradiation. Samples were irradiated for 1 h in the central thimble of the U.S. Geological Survey TRIGA reactor in Denver, Colorado (Dalrymple et al., 1981), at a power level of 1 MW.

After irradiation, monitor minerals were analyzed by total fusion using a CO_2 laser and mass spectrometer at the U.S. Geological Survey in Menlo Park, California. Groundmass samples were removed from their Al package and rewrapped in degassed Ta foil before analysis. For incremental heating analysis of separates, the argon was extracted in discrete temperature steps using a diode laser attached to a MAP216 or Isotopx NGX-600 mass spectrometer. Temperatures were monitored using an optical pyrometer. Before measurement of Ar isotopic composition, groundmass separates were degassed at 400 °C. Extracted Ar was exposed to a 4 A tungsten filament, 125 K cold finger, and two getters (one operated at 300 °C and one at room temperature) to remove active gases. Instrumental mass discrimination was calculated by repeated measurement of atmospheric argon, assuming a $^{40}Ar/^{36}Ar_{atmosphere}$ ratio = 298.56 ± 0.31 (Lee et al., 2006). The $^{40}Ar/^{39}Ar$ ages were calculated

TABLE 2. SIMILARITY COEFFICIENTS FOR TETHEROW BASALT GEOCHEMICAL SAMPLES

Field sample ID	Label	Fulton Ridge						Oak Springs		Tetherow Butte											
		1H	2H	3H	3M	4M	5M	6H	7H	8H	9H	10H	11H	12M	13H	14H	14M	15H	16H	17H	18Ha	18Hb	19H
Fulton Ridge																							
JEO_09-24-2014-08(1)	1H	1																					
JEO 10-15-2020-1(1)	2H	0.96	1																				
JEO_06-15-2016-04(1)	3H	0.98	0.95	1																			
JEO_06-15-2016-04(1)	3M	0.97	0.94	0.98	1																		
04.26.2016.08	4M	0.96	0.94	0.96	0.95	1																	
06.14.2016.18(1)	5M	0.96	0.95	0.98	0.97	0.95	1																
JEO 10-15-2020-2(1)	6H	0.95	0.92	0.96	0.95	0.96	0.95	1															
Oak Springs																							
S20-M2159	7H	0.94	0.92	0.95	0.94	0.95	0.94	0.98	1														
S20-M2160	8H	0.94	0.93	0.96	0.95	0.96	0.96	0.98	0.98	1													
Tetherow Butte																							
S21-M2321	9H	0.96	0.94	0.97	0.96	0.98	0.96	0.96	0.96	0.97	1												
JEO 10-14-2020-2(1)	10H	0.94	0.93	0.95	0.94	0.96	0.95	0.97	0.97	0.99	0.97	1											
S21-M2302	11H	0.96	0.94	0.97	0.96	0.97	0.96	0.97	0.97	0.98	0.98	0.97	1										
CMC20181006	12M	0.93	0.92	0.95	0.95	0.95	0.96	0.95	0.95	0.96	0.95	0.96	0.96	1									
JEO 10-13-2020-7(1)	13H	0.97	0.94	0.97	0.96	0.96	0.96	0.97	0.95	0.96	0.98	0.96	0.98	0.95	1								
JEO 10-13-2020-5(2)	14H	0.92	0.91	0.94	0.94	0.94	0.93	0.95	0.96	0.97	0.95	0.98	0.95	0.95	0.94	1							
10-13-2020-05	14M	0.92	0.92	0.94	0.94	0.95	0.93	0.96	0.96	0.97	0.95	0.98	0.96	0.96	0.94	0.99	1						
S21-M2319	15H	0.94	0.93	0.94	0.95	0.97	0.93	0.94	0.94	0.95	0.96	0.97	0.96	0.95	0.95	0.97	0.97	1					
JEO 10-13-2020-4(1)	16H	0.94	0.93	0.95	0.95	0.97	0.94	0.95	0.95	0.96	0.97	0.97	0.97	0.96	0.95	0.97	0.97	0.99	1				
S21-M2318	17H	0.95	0.93	0.96	0.96	0.98	0.95	0.95	0.95	0.97	0.98	0.98	0.98	0.95	0.96	0.96	0.97	0.98	0.99	1			
JEO 10-13-2020-2(1)	18Ha	0.97	0.96	0.97	0.96	0.96	0.96	0.93	0.94	0.95	0.97	0.95	0.96	0.94	0.95	0.94	0.95	0.96	0.96	0.97	1		
JEO 10-13-2020-2(2)	18Hb	0.96	0.94	0.97	0.95	0.98	0.96	0.98	0.97	0.97	0.99	0.97	0.99	0.96	0.98	0.95	0.95	0.96	0.97	0.98	0.95	1	
JEO 10-13-2020-1(1)	19H	0.95	0.94	0.96	0.95	0.97	0.96	0.95	0.95	0.97	0.98	0.97	0.98	0.96	0.97	0.95	0.96	0.97	0.97	0.98	0.97	0.98	1

Note: Samples were compared using similarity coefficient of Borchardt et al. (1972) to compare concentrations of Si, Ti, Al, Fe, Mn, Mg, Ca, Na, K, and P expressed as oxides with total iron as FeO and normalized to 100% on a volatile-free basis. Numbers in labels are keyed to the map depicted in Figure 1. Labels containing H were analyzed at Hamilton Analytical Lab (Hamilton College, Clinton, New York, USA), and those containing M were analyzed at AGAT Laboratories (Calgary, Alberta, Canada), under contract to the U.S. Geological Survey. Label modifiers a and b refer to duplicate samples from the same site.

using the decay constants recommended by Steiger and Jäger (1977). Uncertainties in reported $^{40}Ar/^{39}Ar$ ages include propagated uncertainties in counting statistics and *J* values.

Findings

The two basalt samples from Dalles basin resulted in complicated argon-release patterns characteristic of argon recoil (e.g., Fleck et al., 2014), with plateaus that showed decreasing age with increasing temperature and inverse isochron diagrams that showed clockwise rotations with increasing temperature (Figs. 13A and 13B). Despite having complicated argon-release patterns, these two samples yielded nearly identical recoil model ages (following Fleck et al., 2014) of 5.43 ± 0.33 Ma (2σ) and 5.43 ± 0.25 Ma. These recoil model ages are our "preferred" interpretation for the argon experiments.

The Tetherow basalt from Deschutes basin [sample JEO-10-13-2020-5(1)] also yielded a complicated argon-release pattern characterized by older ages in the central temperature range of the experiment (600–700 °C) and younger ages at lower and higher temperatures. No robust plateau age could be derived from this sample. An isochron was defined that yielded an age of 5.12 ± 0.05 Ma (2σ) and a trapped $^{40}Ar/^{36}Ar$ ratio of 259.4 ± 9.3 (2σ), which is well below the $^{40}Ar/^{36}Ar$ of atmospheric argon (298.56 ± 0.31; Lee et al., 2006). This isochron age for the Tetherow basalt should be treated with caution, as the low $^{40}Ar/^{36}Ar$ of its trapped gas component suggests this sample may have been affected by argon recoil or experienced mass fractionation during equilibration with the atmosphere.

The two new $^{40}Ar/^{39}Ar$ ages of 5.4 Ma obtained from the Dalles basin Tetherow basalt outcrops in the Fulton Ridge area were slightly older than, but within error of, the 5.17 ± 0.03 Ma (2σ) age for the Tetherow Butte member of the Deschutes Formation reported by Pitcher et al. (2021). They were younger but also within error of the 5.57 ± 0.20 Ma age obtained by Smith et al. (1987) as recalculated by Pitcher et al. (2017). However, the recalculated age of 5.57 ± 0.20 Ma from Smith et al. (1987) is apparently older than the more recent age of 5.17 ± 0.03 Ma from Pitcher et al. (2021), which are both from samples of the Tetherow basalt collected in Deschutes basin. We cannot explain this discrepancy, but taken together, the five $^{40}Ar/^{39}Ar$ assessments and their analytical uncertainties indicate that the basalt erupted between ca. 5.8 Ma and 5.2 Ma. In addition, both the new ages reported here from Dalles basin are consistent with previous age analyses from Deschutes basin.

An additional factor for resolving the age of the Tetherow basalt is its normal polarity. The

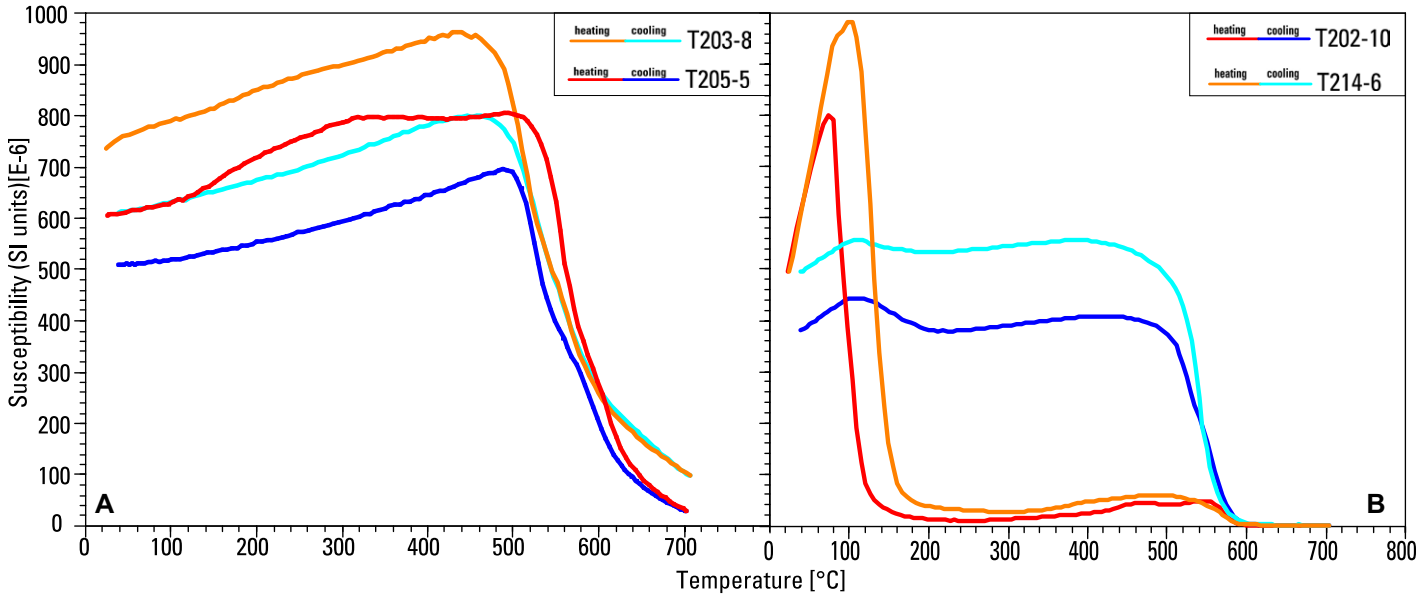

Figure 10. Susceptibility-temperature experiments on powdered specimen material heated in air. Two types of behavior are shown in the panels: (A) lower-titanium titanomagnetite; (B) high-titanium titanomagnetite, indicating quenching of these areas of the flow.

lava flow most likely erupted during the Thvera normal polarity subchron, which lasted from 5.235 Ma to 4.997 Ma (Ogg, 2020). It is less likely—though possible—that the lava erupted during a discrete normal-polarity subchron in chron C3r, which spanned the time 6.023–5.235 Ma (Ogg, 2020). From the polarity timescale consideration, the Tetherow basalt most likely erupted between 5.2 Ma and 5.1 Ma, consistent with the $^{40}Ar/^{39}Ar$ age of 5.17 ± 0.03 Ma reported by Pitcher et al. (2021) as well as the three less precise $^{40}Ar/^{39}Ar$ age analyses reported here.

DISCUSSION

The field characteristics, geochemistry, paleomagnetic orientations, and geochronology provide evidence that the Tetherow basalt flowed the entire length of the early Pliocene Deschutes River valley to the present confluence of the Deschutes and Columbia Rivers (Fig. 1). This conclusion has implications for the regional volcanic, tectonic, and physiographic history, besides raising stratigraphic correlation questions.

Volume, Extent, and Eruption Duration

Both the interbasin travel distance—Deschutes to Dalles—and the intra–Deschutes basin extent of the Tetherow basalt indicate a voluminous sustained eruption. From the Deschutes basin to Fulton Ridge, this lava flow streamed for at least 160 km. The length is unusual: only a few Quaternary lava flows exceed this length (Cashman et al., 1998).

The emplacement of lengthy lava flows requires specific but not extraordinary conditions (Walker, 1973; Cashman et al., 1998, and references therein). A long lava flow requires a substantial eruptive volume emplaced at sustained high rate for the flow not to freeze.

The Tetherow basalt has a volume of 15–20 km^3 bulk rock; a dense-rock equivalent (DRE) volume of ~80% (Lipman and Banks, 1987) is ~12–16 km^3. The estimate confidence is limited because outcrops of the lava flow have been nearly stripped along much of its extent from central Oregon north to the Columbia River. Yet, much of that stretch lies within an ancestral canyon where walls confined the across-canyon breadth of the Tetherow basalt, limiting its impact on the validity of the volume calculation.

The volume range was derived using two approaches: (1) drawing isopachs (lines of equal thickness) and summing resulting area-thickness computations derived by the formula for calculating a frustum (17.0–17.4 km^3) and (2) using the cross sections of Figure 3 to determine a representative cross-sectional area, multiplying the given areal value by the length of the Tetherow basalt's down-valley extent that characterizes the corresponding cross section, and then summing the segment volumes (15.5–19.9 km^3). Each method requires interpretation of flow extent and thickness. For method 1, precision might be improved by increasing the number of thickness measurements and drawing more isopach contours (smaller isopach intervals). For method 2, precision might be improved by increasing the number of cross sections. However, given the uncertainty on the eroded areas of the flow, we consider 12–16 km^3 DRE to be a reasonable volume estimate. This volume compares to lesser flows of flood basalt eruptions and meets or exceeds the volume of several flows within the Saddle Mountains Basalt of the Columbia River Basalt Group (Reidel et al., 2013a).

The eruption rate of the Tetherow basalt lava flow can be deduced from three distinct features: It was a single lava flow through most and possibly all of its 160–180 km length; it has similar outcrop appearance with its tripartite weathering profile (Fig. 6); and it has no evidence of lava tubes. These features indicate a sustained, high extrusion rate. The famous historic (1783) eruption of Lakagigar ("Laki") in Iceland had a high rate of extrusion and produced 10 km^3 (perhaps 7–8 km^3 DRE magma) in only 50 d (Thorarinsson, 1968). The extrusive rate may have varied during the Tetherow basalt eruption, but the Laki volume-time relation requires a long-term average rate of 1850 m^3/s (DRE). A rate of that magnitude could have emplaced the entire Tetherow basalt in 4–6 mo.

Some Hawaiian eruptions have initial extrusion rates that exceed 200 m^3/s, e.g., Mauna Loa's 1975 eruption with 1 d duration and ~280 m^3/s (Lockwood and Lipman, 1987). However, Hawaiian eruptions rapidly slow to rates less than 10 m^3/s. The tubes that develop during these eruptions can feed long lava flows as insulated internal conduits, but long-lived eruptions experience pauses, which lead to tube disruption. When

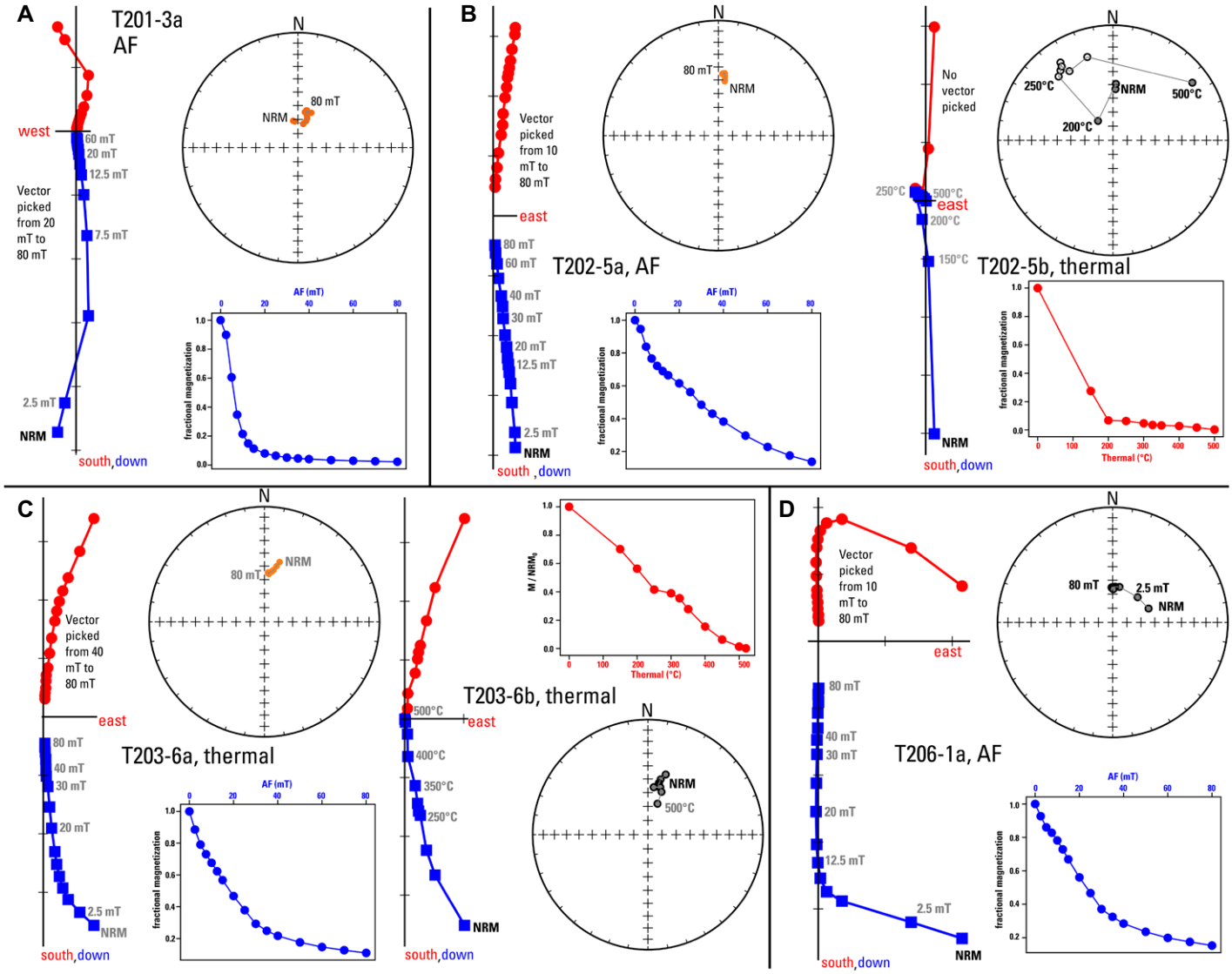

Figure 11. Examples of demagnetization behavior from Tetherow basalt: Zijderveld (1967) diagrams, equal-area plots, and moment-decay diagrams are shown for each example specimen. Paleomagnetic data are shown in geographic coordinates on vector component plots and measurement-level equal-area plots. NRM—natural remanent magnetization. (A) Diagrams for Tetherow basalt at site T201, showing minor secondary component removal during alternating field (AF) demagnetization. (B) Comparison of AF and thermal demagnetization from sister specimens at site T202, with some complexity exhibited during thermal demagnetization. (C) Comparison of AF and thermal demagnetization from sister specimens at site T203, showing identical behavior. (D) Demagnetization diagrams for site T206 on Fulton Ridge, showing removal of secondary component by AF demagnetization. mT—millitesla (peak alternating field used for demagnetization steps).

an eruption resumes, lava breaks out from an obstructed tube to build a flow-on-flow sequence and new tubes. This phenomenon occurred frequently during the 35 yr Pu‘u ‘Ō‘ō eruption at Kīlauea, Hawai‘i (Heliker and Mattox, 2003). Tetherow basalt outcrops, in contrast, lack this flow-on-flow aspect. Lava tubes, whether filled or with head space at the end of an eruption, are recognizable where erosion has exposed the face of the flow. No lava tubes have been recognized among outcrops of the Tetherow basalt.

The Tetherow basalt’s great length and far journey contrast with other basalt flows of similar age that never left Deschutes basin; its large eruptive volume likely played a role. Another major factor was vent proximity to the drainage axis of the Deschutes basin, which provided a ready channel that favored length over lateral spread. The Tetherow basalt interacted with surface water, likely the ancestral Deschutes Rivers, as evidenced by spatter mounds aligned along the probable paleodrainage (Smith, 1986).

Flow within a single channel allowed the Tetherow basalt to approach its maximum potential length, as noted by both models and actual Hawaiian lava flow eruptions (Dietterich and Cashman, 2014). A similar argument, also utilizing paleomagnetic data, explains lengths in excess of 135 km for Pleistocene lava flows within the Grand Canyon (Crow et al., 2015).

Regional Incision and Tectonic Deformation

Incision

The age of the Tetherow basalt (ca. 5.2 Ma) is a datum for assessing incision rates and tectonic deformation (Table S1; Table 5). Regional incision is shown by the position of the base of

TABLE 3. SUMMARY OF PALEOMAGNETIC RESULTS FROM TETHEROW BASALT, NORTH-CENTRAL OREGON

Site	Lat (°N)	Long (°W)	*N*	Dec (°)	Inc (°)	κ	α_{95}
Tetherow basalt							
T201	44.39477	121.19447	7	357.5	58.0	77	6.2
T203	44.6422	121.15138	13	5.6	55.3	203	2.9
T204	44.76535	121.10005	14	8.5	52.9	135	3.5
T211	44.36276	121.22599	9	5.1	54.7	231	3.4
T213	44.82194	121.06892	9	0.1	56.0	350	2.8
T202	44.5458	121.25045	13	6.1	50.0	449	2.0
T212	44.47489	121.2939	8	6.3	50.8	102	5.5
T214	44.72032	121.19572	10	5.0	51.8	163	3.8
Tetherow basalt mean			8	5.0	54.6	440	2.6
Basalt of Fulton Ridge							
T205	45.63972	121.03076	10	5.6	60.3	210	2.9
T206	45.568	120.91425	14	357.5	58.8	198	2.9
T221	45.6378	121.00038	8	10.0	58.3	161	4.5
Basalt of Fulton Ridge mean			3	4.4	59.2	557	5.2
Basalt of Fulton Ridge mean*			3	4.3	58.2	557	5.2

Note: Site—name of cooling unit; Lat—site latitude; Long—site longitude (World Geodetic System 1984 [WGS84] datum); *N*—total number of specimens used in final analysis; Dec—paleomagnetic declination, with mean calculated using circular statistics (Fisher, 1953); Inc—paleomagnetic inclination, with mean calculated using circular statistics (Fisher, 1953); κ—kappa precision parameter (Fisher, 1953); α_{95}—cone of 95% confidence about the mean direction. Basic paleomagnetic data are available in Pivarunas et al. (2023) and the MagIC database (https://doi:10.7288/V4/MAGIC/19605).

*The mean direction was corrected to the common southerly latitude (see text).

the lava flow above the modern river profiles of the Crooked and Deschutes Rivers (Fig. 4). This discussion makes the tacit assumption that the exposed base of basalt is the base of the ancestral river channel. Where this estimation is invalid, the lava base would be placed too shallow, and incision depth and rate would be exaggerated.

In Deschutes basin the base of the Tetherow basalt ranges from ~65 m to 265 m above modern river levels. The low values are near the source vents in the south part of the flow's extent (Fig. 2). The high values characterize the north margin of Deschutes basin. Thus, at river mile 109.5, the Tetherow basalt stands 244 m above modern river level, whereas the Round Butte lava (4.0 ± 0.1 Ma) invaded Deschutes River gravel at 265 m above modern river level (river mile 108; Smith, 1986, p. 174). Some of the downstream profile divergence between Tetherow source vents and river mile 108 may owe to differential incision, but a large part likely is due to both the Crooked and Deschutes River canyons being repeatedly filled by Quaternary lavas from the Newberry area to beyond 44.6°N (Deschutes River mile 109), i.e., the most northern outcrops (Stearns, 1931, p. 145; Smith, 1986, 1987b). The marked steepening of the modern rivers upstream of river mile 114 (Fig. 4) indicates that the Crooked and Deschutes Rivers have not yet fully incised through these young lavas or the adjacent Deschutes Formation to their prior profiles (O'Connor, et al., 2003a). The abundance of resistant pre-Tetherow Oligocene to Miocene lava flows south of Lake Billy Chinook also inhibited Crooked River incision after the Tetherow basalt erupted.

Near Oak Springs, near river mile 47, the Tetherow basalt remnant lies ~220 m above the modern Deschutes River (Fig. 4). West across the river, the extensive basalt of Juniper Flat (2.77 ± 0.36 Ma; R.M. Conrey, Hamilton College, personal commun., cited in Sherrod and

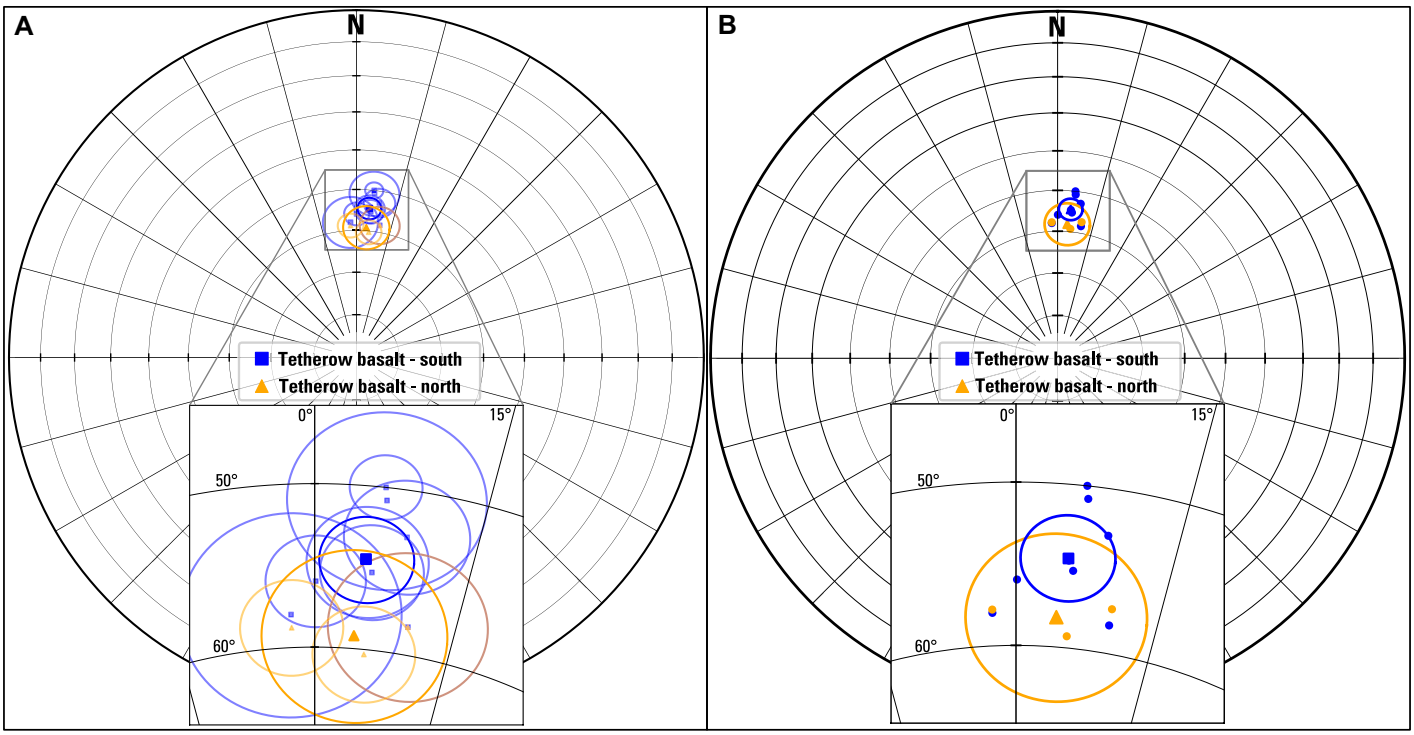

Figure 12. Equal-area diagrams showing site mean paleomagnetic directions. (A) Site-level mean paleomagnetic directions with associated 95% confidence intervals, where southerly sites are shown in blue, and northerly sites (uncorrected to common latitude) are shown in orange, on full equal-area stereonet and with inset. (B) Site-level mean paleomagnetic directions (without associated confidence intervals), with northerly sites (in Dalles basin) corrected to common latitude with southerly sites as discussed in text, on full equal-area stereonet and with inset.

TABLE 4. SUMMARY OF $^{40}Ar/^{39}Ar$ AGES FOR TETHEROW BASALT, NORTH-CENTRAL OREGON, SAMPLES

Sample	Material	Method	Plateau		Isochron			%^{39}Ar [steps]
			Age (Ma) ± 1σ (2σ)	MSWD	Age (Ma) ± 1σ (2σ)	MSWD	$^{40}Ar/^{36}Ar$(i) ± 2σ	
JEO-10-13-2020-5(1)	Groundmass	Diode-IH	4.932 ± 0.044 (0.114)	32.4	**5.123 ± 0.016 (0.051)**	1.84	259.4 ± 9.3	58.5 [600 to 950]
JEO-9-24-14-08 (preferred)	Groundmass	Diode-IH	**5.43 ± 0.1 (0.33)***	117.48	5.02 ± 0.26 (3.36)	42.31	585.3 ± 2520.7	69.4 [600 to 750]
JEO-12-21-17-03 (preferred)	Groundmass	Diode-IH	**5.431 ± 0.09 (0.25)***	93.64	10.8 ± 6 (25.6)	52.92	–6077.6 ± 227007.6	65.6 [600 to 750]
JEO-9-24-14-08 (option 2)	Groundmass	Diode-IH	5.164 ± 0.047 (0.15)	7.4	**5.242 ± 0.023 (0.284)**	0.69	270.1 ± 72.3	26 [750 to 1000]
JEO-12-21-17-03 (option 2)	Groundmass	Diode-IH	5.172 ± 0.052 (0.143)	12.2	**5.273 ± 0.019 (0.079)**	2.12	247.4 ± 28.5	30.1 [700 to 950]

Note: Two different interpretations of $^{40}Ar/^{39}Ar$ experiments for samples JEO-9-21-14-08 and JEO-12-21-17-03 are presented. The age in bold is the preferred interpretation (see text). Steps in last column refer to temperature steps in °C. Additional geochronological data are available in Pivarunas et al. (2023). IH—incremental heating; MSWD—mean square of weighted deviates.

*Recoil model age calculated following Fleck et al. (2019).

Scott, 1995) crops out atop a geochemically similar thick sequence of hyaloclastite, showing that the basalt of Juniper Flat invaded the Deschutes River. The base of the hyaloclastite stands 85 m above modern river level, registering an intermediate river elevation at ca. 2.8 Ma.

In Dalles basin, the base of the Tetherow basalt lies 265 m above the Deschutes River at river mile 5. Near the farthest downstream extent of the Tetherow basalt, at Columbia River mile 198, its base stands ~350 m above preimpoundment Columbia River level. This higher value likely is due to uplift of the north flank of the Dalles-Umatilla syncline (Fig. 5). The basalt of Gordon Butte (0.921 ± 0.014 Ma), which sits atop unweathered Deschutes River gravel 17.2 m above the modern river level (O'Connor et al., 2003a, 2021a), registers an intermediate river elevation at ca. 0.9 Ma.

These positions of the Tetherow basalt indicate regional net incision at rates of 13–67 m per million years (m/m.y.) since 5.2 Ma (Table 5). The smaller values upstream of Deschutes River mile 108 probably show effects of Quaternary lava flows filling the canyon. Net incision rates calculated using the Tetherow basalt position at five sites between river mile 108 and the Columbia River (Table 5: data rows 5–11, nonitalicized rows) range from 42 m/m.y. to 67 m/m.y. For the Fulton Ridge sites, net incision rates of 51–67 m/m.y. likely approximate rock uplift rates because of the near-sea-level elevation (~40 m relative to North American Vertical Datum of 1988 [NAVD88]) of the preimpoundment Deschutes River and Columbia River confluence. This regional incision behind the volcanic arc, though at rates much lower than the ~300 m/m.y. for the axis of the Cascade Range at the latitude of the Columbia River (O'Connor et al., 2021a), explains the deeply incised rivers and broad plateau physiography of the region.

We found that incision along the path of the lava flow has slowed through time, whereas most incision may have taken place between 5 Ma and 4 Ma and ca. 1 Ma. The similar relative positions of the Tetherow basalt (ca. 5.2 Ma) and Round Butte basalt (ca. 4 Ma) near Round Butte Dam indicate little incision—perhaps even local deposition—in the millennia between these lavas. In addition, the presence of lava flows from the Newberry area near present river elevation in the southern Deschutes basin indicates little net incision in the past 1.2 m.y. (O'Connor et al., 2003b). Near Oak Springs, the position of hyaloclastite (ca. 2.8 Ma) relative to the Tetherow basalt implies 61 m/m.y. of net incision between

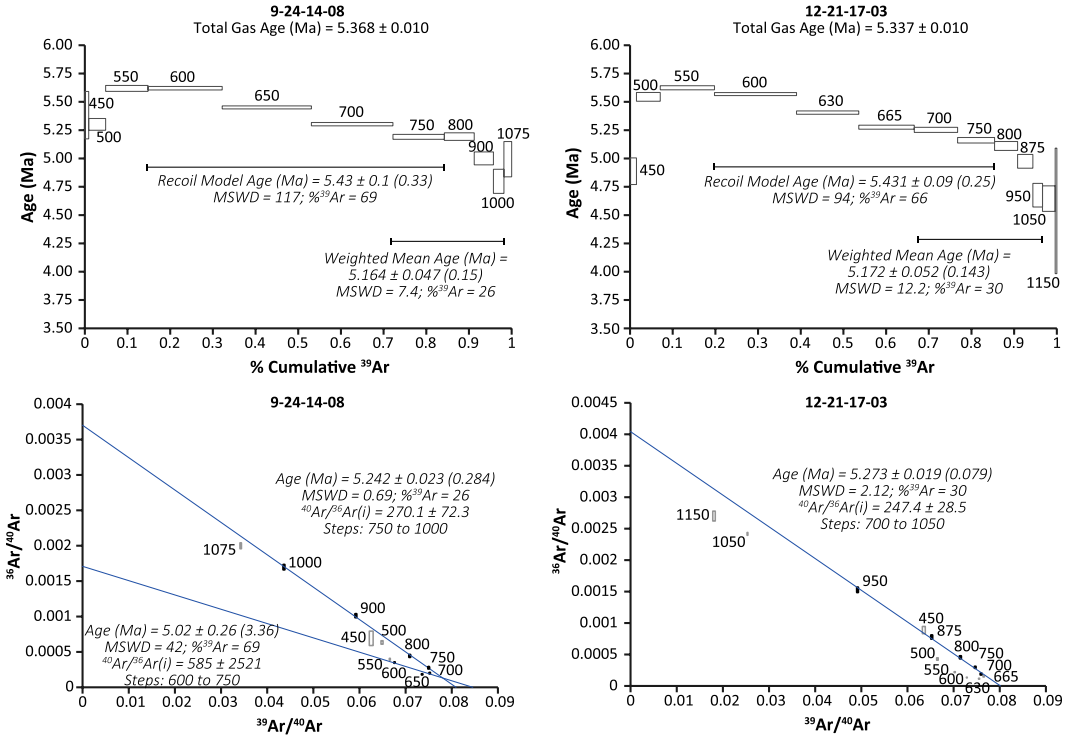

Figure 13. Age spectrum and isochron diagrams for samples of the Tetherow basalt from the Fulton Ridge area. Box heights represent the 1σ age uncertainty for each temperature step. A recoil model age using the central ~70% of the age spectrum, following Fleck et al. (2014), and an age calculated using the high-temperature steps are presented for each sample. Both samples showed identical argon release patterns and yielded identical ages. The isochron corresponding to the recoil model age of sample JEO-12-21-17-03 is not shown because it yielded a positive slope. The positive slope is due to the counterclockwise rotation of the argon isotope composition in inverse isochron space, likely due to argon recoil during irradiation of these fine-grained samples. Reported uncertainties for trapped gas compositions, or $^{40}Ar/^{36}Ar$(i), are 2σ. Reported ages are in the following format: Age ± 1σ (2σ). MSWD—mean square of weighted deviates.

TABLE 5. REGIONAL INCISION CALCULATIONS FROM TETHEROW BASALT POSITION

River mile	River geographic	River elevation (m [ft])	Lava base (m [ft])	Incision (m)	Rate (m/m.y.)
C18.5	Highway 97 bridge	770 [2470]	835 [2680]	65	13
C5	S. end Lake Billy Chinook	573 [1880]	792 [2600]	219	42
109.5	Just below Round Butte Dam	463 [1520]	707 [2320]	244	47
*108**	*Just below Round Butte Dam*	*454 [1490]*	*719 [2360]*	*265*	*66*
	Warm Springs Grade	426 [1397]	661 [2170]	235	45
87	Trout Creek confluence	390 [1280]	655 [2149]	265	51
47	Oak Springs	237	457	220	42
*47**	*Oak Springs*	*237*		*85*	*30*
5	S. of Freebridge	65	330	265	51
*5**	*S. of Freebridge*	*65*	*82*	*17*	*18*
CR198	Lake Celilo	25	375	350	67

Note: Regional incision rate calculations are from modern river elevation and Tetherow basalt's lower contact elevation. All elevations are relative to sea level. Additional field station data bearing on incision rate calculations are available in Pivarunas et al. (2023).

*Entries in italics with asterisks in river mile column are incision rate calculations from units other than the Tetherow basalt (see text).

5.2 Ma and 2.8 Ma, whereas the post–2.8 Ma net incision rate decreased by about half (~30 m/m.y.). Likewise, at Fulton Ridge, the Tetherow basalt defines an overall post–5.2 Ma net incision rate of 51 m/m.y., and the basalt of Gordon Butte defines a net incision rate of ~18 m/m.y. The post–1 Ma incision estimate is a third of the overall post–5.2 Ma rate indicated by the nearby Tetherow basalt. The Gordon Butte lava datum also indicates an incision rate of 58 m/m.y. during the 4.3 m.y. between 5.2 Ma and 0.9 Ma near the Columbia River confluence.

Tectonic Deformation

The Tetherow basalt crossed several structures over its 160 km northward flow path, including east-west–oriented folds encompassing the southern part of the Yakima fold belt and northwest-oriented strike-slip faults related to regional dextral shear (Wells et al., 1998; Anderson et al., 2013; Wells and McCaffrey, 2013). Some of the overall divergence between the Tetherow basalt gradient and modern river profile may be due to deformation on such structures, but evidence for deformation is most compelling in the Fulton Ridge area (Fig. 5). There, the Tetherow basalt appears to be deformed by both the Dalles-Umatilla syncline (Newcomb, 1967, 1969) and the strike-slip Laurel fault (Anderson et al., 2013). Anderson et al. (2013) suggested 250–350 m of right-lateral offset of the paleodrainage traced by the Tetherow basalt as it crosses the trace of the Laurel fault. However, given the curvilinear trace of the Tetherow basalt's path along Fulton Ridge, we found the maximum lateral separation to lie at the low end of this estimation, ~250 m, and actual separation could be substantially less. If expressed as deformation since 5.2 Ma, the maximum rate of separation is ~50 m/m.y. or perhaps much less.

Deformation within the Dalles-Umatilla syncline is also demonstrated by the elevation of the top of the Tetherow basalt (Fig. 5), which must initially have been a planar and gently down-valley-sloping surface. About 400 m north of where the flow crosses the axis of the syncline as mapped by Newcomb (1969), the basalt top has an elevation of 330 m (site 5 on Fig. 5; station JEO 06-14-2016-18; Table S4). North from there, on the rising north limb of the syncline, the surface of the basalt gains elevation despite being in the down-flow direction, reaching its highest elevation of 384 m (station JEO 09-24-2014-08; Fig. 5, numerical label 1) 2.8 km north of the syncline axis. This indicates at least 54 m of uplift, and likely more, since this difference does not account for the ~2 m/km lava-flow gradient (Fig. 5) over the ~8 km flow distance between sites. Total vertical deformation therefore reaches as much as 70 m. This equates to 1.4° of southward tilt, measured over the 2.4 km distance orthogonal to the syncline axis. Anderson et al. (2013, p. 341) stated that the underlying Columbia River Basalt Group (ca. 16 Ma) dips south at ~4° here, indicating that the post–5.2 Ma deformation has continued at about the same rate, ~0.25°/m.y., shown by the Columbia River Basalt Group. This deformation of the Tetherow basalt in the Fulton Ridge area shows that both the Laurel fault and the Dalles-Umatilla syncline were active for long periods, serving as structures that accommodated regional strain, clockwise rotation, and north-south compression, even if regional uplift has slowed.

River History

Outcrops of the Tetherow basalt show that the Deschutes River existed in central Oregon since before ca. 5.2 Ma. The river's position today is in part a legacy of the Tetherow basalt eruption. The present-day track of the Deschutes River is primarily west of the Tetherow lava extent, where the river incised along the edge of the resistant lava flow.

The position of the Tetherow basalt in relation to Dalles Formation strata shows that the Columbia River had not yet occupied Dalles basin at ca. 5.2 Ma, the time of the Tetherow eruption. The Dalles Formation, which underlies the basalt, is composed of two distinct facies within Dalles basin: (1) a volcaniclastic sequence, derived from volcanic centers to the southwest (ca. 9–5 Ma), composed of tuff, tuffaceous sandstone, and tuffaceous diamict that form an apron sloping, thinning, and fining northeast (Newcomb, 1966; McClaughry et al., 2020, 2021b), and (2) a fluvial wedge of conglomerate and sandstone deposited by west- and northwest-flowing rivers running along the Dalles-Umatilla syncline (Newcomb, 1966). The two facies interfinger west of the Deschutes River mouth (Newcomb, 1966). However, clasts of the fluvial facies are entirely of types sourced from the present John Day and Deschutes River basins (Newcomb, 1966; O'Connor et al., 2021b). The Dalles Formation contains no clasts—quartzite, metamorphic rock, or granitic rock—that would indicate Columbia or Snake River affinity. This contrasts with suggestions (Reidel et al., 2013b) that the Snake River flowed through the Umatilla-Dalles basins in Pliocene time. Neither the Columbia River nor the Snake River flowed through Dalles basin until sometime after the ca. 5.2 Ma emplacement of the Tetherow basalt. Instead, quartzite-rich Miocene gravels of Columbia River type trace a route north of the Columbia Hills anticline (Fig. 1; Newcomb, 1969; O'Connor et al., 2021b). The oldest Columbia River gravel yet found in Dalles basin lies beneath a basalt (ca. 0.83 Ma) near river level on Miller Island (Fig. 5) near the Deschutes-Columbia confluence (O'Connor et al., 2021a), showing that the Columbia River did not enter Dalles basin until between 5.2 Ma and 0.83 Ma.

CONCLUSIONS

The Tetherow basalt is one of the longest non-flood-basalt lava flows yet recognized, reaching 160–180 km from its source vents at ca. 5.2 Ma. The Tetherow basalt's geochemistry is unique within its basin of origin; unlike other Deschutes basin lava, the Tetherow is high in iron, like Columbia River Basalt Group flows. Its volume is large, reaching the size of late-stage hotspot lava flows like the Saddle Mountains Basalt of the Columbia River Basalt Group. The Tetherow basalt had a very high discharge rate to sustain its emplacement for well over 100 km, although it was aided in this by the channelization of the river canyon. Together, these observations indicate that the Tetherow basalt resembles lava of the Columbia River Basalt Group flood basalts.

Our results showed that a combined observational-analytical approach facilitates correlation of long-distance lava flows in the absence of

continuous outcrops. The Tetherow basalt presented difficulty in obtaining coherent radiometric ages, illustrating the importance of field, geochemical, and paleomagnetic techniques to best establish the correlation. Unique geochemistry and the trace of the lava path, where preserved, may be the best indicators for correlating Tetherow basalt outcrops. The substantial volume of the eruption as well as the geographic setting of the Tetherow vents near the Deschutes basin axial drainage affected the unusual length of this flow. The present-day above-river elevation of the lava flow allows estimation of regional incision rates, and later volcanic episodes show how incision rates have changed through time. The Tetherow basalt managed to thread its way north into Dalles basin and may provide a datum for the cessation of Dalles Formation deposition.

ACKNOWLEDGMENTS

This study benefited from conversations with Rick Conrey, Ray Wells, Duane Champion, and Gary Smith. Rick Conrey first proposed the possible correlation. Gary Smith and Jason McClaughry both provided excellent reviews, which improved this paper. Nancy Stamm provided a helpful review that improved readability and assessed geologic names. An anonymous reviewer and the associate editor also provided useful reviews. We thank Phil Kaser, Martin Underhill, and Jim Markman for permission to sample outcrops in Dalles basin. Any use of trade, firm, or product names is for descriptive purposes only and does not imply endorsement by the U.S. government. Data underlying this paper are available at https://doi:10.5066/P9R73C3D. They are also available in the Supplemental Material. Table S1 contains field stations and observations, Tables S2 and S3 contain trace-element data from sites where major-element chemistry is reported in Table 1 in the paper. Table S4 contains $^{40}Ar/^{39}Ar$ data. Paleomagnetic data are retained in the MagIC database (https://doi:10.7288/V4/MAGIC/19605).

REFERENCES CITED

Anderson, J.L., Tolan, T.L., and Wells, R.E., 2013, Strike-slip faults in the western Columbia River flood basalt province, Oregon and Washington, *in* Reidel, S.P., Camp, V.E., Ross, M.E., Wolff, J.A., Martin, B.S., Tolan, T.L., and Wells, R.E., eds., The Columbia River Flood Basalt Province: Geological Society of America Special Paper 497, p. 325–347, https://doi.org/10.1130/2013.2497(13).

Arculus, R.J., 2003, Use and abuse of the terms calcalkaline and calcalkalic: Journal of Petrology, v. 44, no. 5, p. 929–935, https://doi.org/10.1093/petrology/44.5.929.

Bacon, C.R., Bruggman, P.E., Christiansen, R.L., Clynne, M.A., Donnelly-Nolan, J.M., and Hildreth, W., 1997, Primitive magmas at five Cascade volcanic fields: Melts from hot, heterogeneous sub-arc mantle: Canadian Mineralogist, v. 35, no. 2, p. 397–423.

Bogue, S.W., and Coe, R.S., 1981, Paleomagnetic correlation of Columbia River basalt flows using secular variation: Journal of Geophysical Research: Solid Earth, v. 86, p. 11,883–11,897, https://doi.org/10.1029/JB086iB12p11883.

Böhnel, H., and Schnepp, E., 1999, Precision of the paleomagnetic method: An example from the Quaternary Eifel volcanics (Germany): Earth, Planets, and Space, v. 51, no. 6, p. 403–412, https://doi.org/10.1186/BF03352244.

Borchardt, G.A., Aruscavage, P.J., and Millard, H.T., 1972, Correlation of the Bishop Ash, a Pleistocene marker bed, using instrumental neutron activation analysis: Journal of Sedimentary Research, v. 42, no. 2, p. 301–306, https://doi.org/10.1306/74D72527-2B21-11D7-8648000102C1865D.

Bowman, J.D., Czajkowski, J.L., Reidel, S.P., Boschmann, D.E., and Fusso, L.A., 2015, Washington State Rock Geochemistry Database—GIS Data: Washington Division of Geology and Earth Resources Digital Data Series 5, Version 1.1, originally released October 2014, https://fortress.wa.gov/dnr/geologydata/publications/data_download/ger_portal_geochemistry.zip.

Butler, R.F., 1992, Paleomagnetism: Magnetic Domains to Geologic Terranes: Boston, Massachusetts, Blackwell Scientific Publications, 238 p.

Cannon, C.M., and O'Connor, J.E., 2019, New constraints on the timing of Neogene filling and incision of the Dalles basin, Oregon and Washington: Geological Society of America Abstracts with Programs, v. 51, no. 4, https://doi.org/10.1130/abs/2019CD-329350.

Carlson, R.W., Grove, T.L., and Donnelly-Nolan, J.M., 2018, Origin of primitive tholeiitic and calc-alkaline basalts at Newberry Volcano, Oregon: Geochemistry, Geophysics, Geosystems, v. 19, no. 4, p. 1360–1377, https://doi.org/10.1029/2018GC007454.

Cashman, K., Pinkerton, H., and Stephenson, J., 1998, Introduction to special section: Long lava flows: Journal of Geophysical Research: Solid Earth, v. 103, no. B11, p. 27,281–27,289, https://doi.org/10.1029/98JB01820.

Conrey, R.M., Sherrod, D.R., Hooper, P.R., and Swanson, D.A., 1997, Diverse primitive magmas in the Cascade arc, northern Oregon and southern Washington: Canadian Mineralogist, v. 35, no. 2, p. 367–396.

Conrey, R.M., Hooper, P.R., Larson, P.B., Chesley, J., and Ruiz, J., 2001, Trace element and isotopic evidence for two types of crustal melting beneath a High Cascade volcanic center, Mt. Jefferson, Oregon: Contributions to Mineralogy and Petrology, v. 141, no. 6, p. 710–732, https://doi.org/10.1007/s004100100259.

Conrey, R.M., Grunder, A.L., and Schmidt, M.E., 2004, SOTA Field Trip Guide: State of the Cascade Arc: Stratocone Persistence, Mafic Lava Shields, and Pyroclastic Volcanism Associated with Intra-Arc Rift Propagation: Oregon Department of Geology and Mineral Industries Open-File Report O-04-04, 39 p., https://www.oregongeology.org/pubs/ofr/O-04-04.pdf.

Cox, A., 1961, Anomalous Remanent Magnetization of Basalt: U.S. Geological Survey Bulletin 1083-E, p. 131–160, https://pubs.usgs.gov/bul/1083e/report.pdf.

Crow, R.S., Karlstrom, K.E., Mcintosh, W., Peters, L., Crossey, L., and Eyster, A., 2015, A new model for Quaternary lava dams in Grand Canyon based on $^{40}Ar/^{39}Ar$ dating, basalt geochemistry, and field mapping: Geosphere, v. 11, p. 1305–1342, https://doi.org/10.1130/GES01128.1.

Dalrymple, G.B., Alexander, E.C., Jr., Lanphere, M.A., and Kraker, G.P., 1981, Irradiation of Samples for $^{40}Ar/^{39}Ar$ Dating Using the Geological Survey TRIGA Reactor: U.S. Geological Survey Professional Paper 1176, 55 p., https://doi.org/10.3133/pp1176.

Dietterich, H.R., and Cashman, K.V., 2014, Channel networks within lava flows: Formation, evolution, and implications for flow behavior: Journal of Geophysical Research: Earth Surface, v. 119, no. 8, p. 1704–1724, https://doi.org/10.1002/2014JF003103.

Doell, R.R., and Cox, A.V., 1963, The accuracy of the paleomagnetic method as evaluated from historic Hawaiian lava flows: Journal of Geophysical Research, v. 68, p. 1997–2009, https://doi.org/10.1029/JZ068i007p01997.

Dunlop, D.J., and Özdemir, Ö., 2001, Rock Magnetism: Fundamentals and Frontiers: Cambridge, UK, Cambridge University Press, 565 p.

Fisher, R.A., 1953, Dispersion on a sphere: Proceedings of the Royal Astronomical Society of London, v. 217, p. 295–305, https://doi.org/10.1098/rspa.1953.0064.

Fleck, R.J., Hagstrum, J.T., Calvert, A.T., Evarts, R.C., and Conrey, R.M., 2014, $^{40}Ar/^{39}Ar$ geochronology, paleomagnetism, and evolution of the Boring volcanic field, Oregon and Washington, USA: Geosphere, v. 10, p. 1283–1314, https://doi.org/10.1130/GES00985.1.

Fleck, R.J., Calvert, A.T., Coble, M.A., Wooden, J.L., Hodges, K., Hayden, L.A., van Soest, M.C., du Bray, E.A., and John, D.A., 2019, Characterization of the rhyolite of Bodie Hills and $^{40}Ar/^{39}Ar$ intercalibration with Ar mineral standards: Chemical Geology, v. 525, p. 282–302, https://doi.org/10.1016/j.chemgeo.2019.07.022.

GEOROC/DIGIS Team, 2020, GEOROC: https://georoc.eu/ (accessed 2020).

Gill, J.B., 1981, Orogenic Andesites and Plate Tectonics: Berlin, Springer-Verlag, 392 p., https://doi.org/10.1007/978-3-642-68012-0.

Hagstrum, J.T., and Champion, D.E., 1994, Paleomagnetic correlation of late Quaternary lava flows in the lower east rift zone of Kilauea Volcano, Hawaii: Journal of Geophysical Research: Solid Earth, v. 99, no. B11, p. 21,679–21,690, https://doi.org/10.1029/94JB01852.

Heliker, C.C., and Mattox, T.N., 2003, The first two decades of the Pu'u 'Ō'ō–Kūpaianaha eruption: Chronology and selected bibliography, *in* Heliker, C.C., Swanson, D.A., and Takahashi, T.J., eds., The Pu'u 'Ō'ō-Kūpaianaha Eruption of Kīlauea Volcano, Hawai'i: The First 20 Years: U.S. Geological Survey Professional Paper 1676, p. 1–27, https://pubs.usgs.gov/pp/pp1676/pp1676_01.pdf.

Heslop, D., and Roberts, A.P., 2018, Revisiting the paleomagnetic reversal test: A Bayesian hypothesis testing framework for a common mean direction: Journal of Geophysical Research: Solid Earth, v. 123, p. 7225–7236, https://doi.org/10.1029/2018JB016081.

Hildreth, W., and Fierstein, J., 2015, Geologic Map of the Simcoe Mountains Volcanic Field, Main Central Segment, Yakama Nation, Washington: U.S. Geological Survey Scientific Investigations Map 3315, scale 1:24,000, https://doi.org/10.3133/sim3315.

Holcomb, R., Champion, D.E., and McWilliams, M., 1986, Dating recent Hawaiian lava flows using paleomagnetic secular variation: Geological Society of America Bulletin, v. 97, p. 829–839, https://doi.org/10.1130/0016-7606(1986)97<829:DRHLFU>2.0.CO;2.

Hughes, S.S., 1990, Mafic magmatism and associated tectonism of the central High Cascade Range, Oregon: Journal of Geophysical Research: Solid Earth, v. 95, no. B12, p. 19,623–19,638, https://doi.org/10.1029/JB095iB12p19623.

Irvine, T.N., and Baragar, W.R.A., 1971, A guide to the chemical classification of the common volcanic rocks: Canadian Journal of Earth Sciences, v. 8, no. 5, p. 523–548, https://doi.org/10.1139/e71-055.

Kirschvink, J.L., 1980, The least-squares line and plane and the analysis of palaeomagnetic data: Geophysical Journal International, v. 62, p. 699–718, https://doi.org/10.1111/j.1365-246X.1980.tb02601.x.

Lee, J.Y., Marti, K., Severinghaus, J.P., Kawamura, K., Yoo, H.S., Lee, J.B., and Kim, J.S., 2006, A redetermination of the isotopic abundances of atmospheric Ar: Geochimica et Cosmochimica Acta, v. 70, no. 17, p. 4507–4512, https://doi.org/10.1016/j.gca.2006.06.1563.

Leeman, W.P., Lewis, J.F., Evarts, R.C., Conrey, R.M., and Streck, M.J., 2005, Petrologic constraints on the thermal structure of the Cascades arc: Journal of Volcanology and Geothermal Research, v. 140, no. 1–3, p. 67–105, https://doi.org/10.1016/j.jvolgeores.2004.07.016.

Le Maitre, R.W., ed., 2002, Igneous Rocks: A Classification and Glossary of Terms: Cambridge, UK, Cambridge University Press, 236 p., https://doi.org/10.1017/CBO9780511535581.

Lipman, P.W., and Banks, N.G., 1987, A'a flow dynamics, Mauna Loa 1984, *in* Decker, R.W., Wright, T.L., and Stauffer, P.H., eds., Volcanism in Hawaii: U.S. Geological Survey Professional Paper 1350, p. 1527–1567, http://pubsdata.usgs.gov/pubs/pp/1987/1350/index.html.

Lockwood, J.P., and Lipman, P.W., 1987, Holocene eruptive history of Mauna Loa volcano, *in* Decker, R.W., Wright, T.L., and Stauffer, P.H., eds., Volcanism in Hawaii: U.S. Geological Survey Professional Paper 1350, p. 509–535, http://pubsdata.usgs.gov/pubs/pp/1987/1350/index.html.

Madin, I.P., and McClaughry, J.D., 2019, Geologic Map of the Biggs Junction and Rufus 7.5′ Quadrangles, Sherman and Gilliam Counties, Oregon: Oregon Department of Geology and Mineral Industries Geologic Map

Series GMS-124, scale 1:24,000, https://www.oregongeology.org/pubs/gms/p-GMS-124.htm.

McClaughry, J.D., Wiley, T.J., Conrey, R.M., Jones, C.B., and Lite, K.E., 2012, Digital Geologic Map of the Hood River Valley, Hood River and Wasco Counties, Oregon: Oregon Department of Geology and Mineral Industries Open-File Report O-12-03, 130 p., https://www.oregongeology.org/pubs/ofr/p-O-12-03.htm.

McClaughry, J.D., Scott, W.E., Duda, C.J.M., and Conrey, R.M., 2020, Geologic Map of the Dog River and Northern Part of the Badger Lake 7.5′ Quadrangles, Hood River County, Oregon: Oregon Department of Geology and Mineral Industries Geologic Map Series GMS-126, scale 1:24,000, https://www.oregongeology.org/pubs/gms/p-GMS-126.htm.

McClaughry, J.D., Ferns, M.L., and Gordon, C.L., 2021a, Geology of the North Half of the Lower Crooked River Basin, Crook, Deschutes, Jefferson, and Wheeler Counties, Oregon: Oregon Department of Geology and Mineral Industries Bulletin 108, 286 p., https://pubs.oregon.gov/dogami/B/B108/Bulletin%20-108_Plate.pdf.

McClaughry, J.D., Herinckx, H.H., Niewendorp, C.A., Azzopardi, C.J.M., and Hackett, J.A., 2021b, Geologic Map of the Dufur Area, Wasco County, Oregon: Oregon Department of Geology and Mineral Industries Geologic Map Series GMS-127, scale 1:24,000, https://www.oregongeology.org/pubs/gms/p-GMS-127.htm.

McFadden, P.L., and Lowes, F.J., 1981, The discrimination of mean directions drawn from Fisher distributions: Geophysical Journal International, v. 67, p. 19–33, https://doi.org/10.1111/j.1365-246X.1981.tb02729.x.

McFadden, P.L., and McElhinny, M.W., 1990, Classification of the reversal test in palaeomagnetism: Geophysical Journal International, v. 103, no. 3, p. 725–729, https://doi.org/10.1111/j.1365-246X.1990.tb05683.x.

Miyashiro, A., 1974, Volcanic rock series in island arcs and active continental margins: American Journal of Science, v. 274, p. 321–355, https://doi.org/10.2475/ajs.274.4.321.

Newcomb, R.C., 1966, Lithology and eastward extension of the Dalles Formation, Oregon and Washington, *in* Geological Survey Research 1966, Chapter D: U.S. Geological Survey Professional Paper 550-D, p. D59–D63, https://doi.org/10.3133/pp550D.

Newcomb, R.C., 1967, The Dalles-Umatilla syncline, Oregon and Washington, *in* Geological Survey Research 1967, Chapter B: U.S. Geological Survey Professional Paper 575-B, p. B88–B93, https://doi.org/10.3133/pp575B.

Newcomb, R.C., 1969, Effect of Tectonic Structure on the Occurrence of Ground Water in the Basalt of the Columbia River Group of The Dalles Area, Oregon and Washington: U.S. Geological Survey Professional Paper 383C, 33 p., https://doi.org/10.3133/pp383C.

O'Connor, J.E., Curran, J.H., Beebee, R.A., Grant, G.E., and Sarna-Wojcicki, A., 2003a, Quaternary geology and geomorphology of the lower Deschutes River canyon, Oregon, *in* O'Connor, J.E., and Grant, G.E., eds., A Peculiar River—Geology, Geomorphology, and Hydrology of the Deschutes River, Oregon: American Geophysical Union Water Science and Application Series 7, p. 73–94, https://doi.org/10.1029/WS007.

O'Connor, J.E., Grant, G.E., and Haluska, T.L., 2003b, Overview of geology, hydrology, geomorphology, and sediment budget of the Deschutes River basin, Oregon, *in* O'Connor, J.E., and Grant, G.E., eds., A Peculiar River—Geology, Geomorphology, and Hydrology of the Deschutes River, Oregon: American Geophysical Union Water Science and Application Series 7, p. 7–29, https://doi.org/10.1029/WS007.

O'Connor, J.E., Wells, R.E., Bennett, S.E., Cannon, C.M., Staisch, L.M., Anderson, J.L., Pivarunas, A.F., Gordon, G.W., Blakely, R.J., Stelten, M.E., and Evarts, R.C., 2021a, Arc versus river—The geology of the Columbia River Gorge, *in* Booth, A.M., and Grunder, A.L., eds., From Terranes to Terrains: Geologic Field Guides on the Construction and Destruction of the Pacific Northwest: Geological Society of America Field Guide 62, p. 131–186, https://doi.org/10.1130/2021.0062(05).

O'Connor, J.E., Cannon, C.M., Schwid, M.F., Staisch, L., Engstrom, J., and Lee, S., 2021b, 10,000 pebbles of the Columbia River basin—A provenance assessment: Geological Society of America Abstracts with Programs, v. 53, no. 6, https://doi.org/10.1130/abs/2021AM-369253.

Ogg, J.G., 2020, Geomagnetic polarity time scale, *in* Gradstein, F.M., Ogg, J.G., Schmitz, M., and Ogg, G., eds., Geologic Time Scale 2020: Amsterdam, Elsevier, p. 159–192, https://doi.org/10.1016/B978-0-12-824360-2.00005-X.

Oregon Water Resources Department, 2020, Groundwater Information System (Geochemistry): https://apps.wrd.state.or.us/apps/gw/gw_info/gw_info_report/gw_search.aspx (accessed 10 April 2020).

Pitcher, B.W., Kent, A.J.R., Grunder, A.L., and Duncan, R.A., 2017, Frequency and volumes of ignimbrite eruptions following the late Neogene initiation of the central Oregon High Cascades: Journal of Volcanology and Geothermal Research, v. 339, p. 1–22, https://doi.org/10.1016/j.jvolgeores.2017.04.019.

Pitcher, B.W., Kent, A.J., and Grunder, A.L., 2021, Tephrochronology of North America's most recent arc-sourced ignimbrite flare-up: The Deschutes Formation of the central Oregon Cascades: Journal of Volcanology and Geothermal Research, v. 412, https://doi.org/10.1016/j.jvolgeores.2021.107193.

Pivarunas, A.F., O'Connor, J.E., Cannon, C.M., Sherrod, D.R., and Stelten, M.E., 2023, Field, Geochemical, Geochronological, and Magnetic Data from a Pliocene Basalt Flow along the Deschutes River in North-Central Oregon: U.S. Geological Survey Data Release, https://doi.org/10.5066/P9R73C3D.

Reidel, S.P., Camp, V.E., Tolan, T.L., Martin, B.S., Ross, M.E., Wolff, J.A., and Wells, R.E., 2013a, The Columbia River flood basalt province—Stratigraphy, areal extent, volume, and physical volcanology, *in* Reidel, S.P., Camp, V.E., Ross, M.E., Wolff, J.A., Martin, B.S., Tolan, T.L., and Wells, R.E., eds., The Columbia River Flood Basalt Province: Geological Society of America Special Paper 497, p. 1–43, https://doi.org/10.1130/2013.2497(01).

Reidel, S.P., Tolan, T.L., Camp, V.E., Ross, M.E., Wolff, J.A., Martin, B.S., and Wells, R.E., 2013b, The late Cenozoic evolution of the Columbia River system in the Columbia River flood basalt province, *in* Reidel, S.P., Camp, V.E., Ross, M.E., Wolff, J.A., Martin, B.S., Tolan, T.L., and Wells, R.E., eds., The Columbia River Flood Basalt Province: Geological Society of America Special Paper 497, p. 201–230, https://doi.org/10.1130/2013.2497(08).

Robinson, P.T., and Stensland, D.E., 1979, Geologic Map of the Smith Rock Area, Jefferson, Deschutes, and Crook Counties, Oregon: U.S. Geological Survey Miscellaneous Investigations Map I-1142, scale 1:48,000. [Author note: incorrectly listed as D.H. Stensland in original publication.]

Rowe, M.C., Kent, A.J.R., and Nielsen, R.L., 2009, Subduction influence on oxygen fugacity and trace and volatile elements in basalts across the Cascade volcanic arc: Journal of Petrology, v. 50, no. 1, p. 61–91, https://doi.org/10.1093/petrology/egn072.

Sawlan, M.G., 2018, Alteration, mass analysis, and magmatic compositions of the Sentinel Bluffs Member, Columbia River flood basalt province: Geosphere, v. 14, p. 286–303, https://doi.org/10.1130/GES01188.1.

Schmidt, M.E., and Grunder, A.L., 2009, The evolution of North Sister: A volcano shaped by extension and ice in the central Oregon Cascade Arc: Geological Society of America Bulletin, v. 121, p. 643–662, https://doi.org/10.1130/B26442.1.

Schmidt, M.E., and Grunder, A.L., 2011, Deep mafic roots to arc volcanoes: Mafic recharge and differentiation of basaltic andesite at North Sister volcano, Oregon Cascades: Journal of Petrology, v. 52, no. 3, p. 603–641, https://doi.org/10.1093/petrology/egq094.

Sherrod, D.R., and Scott, W.E., 1995, Preliminary Geologic Map of the Mount Hood 30- by 60-Minute Quadrangle, Northern Cascade Range, Oregon: U.S. Geological Survey Open-File Report 95-219, scale 1:100,000, https://doi.org/10.3133/ofr95219. [Full-color plate is available as USGS Data Series 906, Digital Data for Preliminary Geologic Map of the Mount Hood 30- by 60-Minute Quadrangle, Northern Cascade Range, Oregon.]

Sherrod, D.R., Taylor, E.M., Ferns, M.L., Scott, W.E., Conrey, R.M., and Smith, G.A., 2004, Geologic Map of the Bend 30- × 60-Minute Quadrangle, Central Oregon: U.S. Geological Survey Geologic Investigations Series Map I-2683, scale 1:100,000, https://doi.org/10.3133/i2683.

Shervais, J.W., 1982, Ti-V plots and the petrogenesis of modern and ophiolitic lavas: Earth and Planetary Science Letters, v. 59, no. 1, p. 101–118, https://doi.org/10.1016/0012-821X(82)90120-0.

Smith, G.A., 1986, Stratigraphy, Sedimentology, and Petrology of Neogene Rocks in the Deschutes Basin, Central Oregon: A Record of Continental-Margin Volcanism and its Influence on Fluvial Sedimentation in an Arc-Adjacent Basin [Ph.D. thesis]: Corvallis, Oregon, Oregon State University, 380 p., https://ir.library.oregonstate.edu/concern/graduate_thesis_or_dissertations/c247dw09t.

Smith, G.A., 1987a, Geologic Map of the Madras West and Madras East Quadrangles, Jefferson County, Oregon: Oregon Department of Geology and Mineral Industries Geologic Map Series GMS-45, scale 1:24,000, https://www.oregongeology.org/pubs/gms/GMS-045.pdf.

Smith, G.A., 1987b, Geologic Map of the Seekseequa Junction and a Portion of the Metolius Bench Quadrangles, Jefferson County, Oregon: Oregon Department of Geology and Mineral Industries Geologic Map Series GMS-44, scale 1:24,000, https://www.oregongeology.org/pubs/gms/GMS-044.pdf.

Smith, G.A., and Hayman, G.A., 1987, Geologic Map of the Eagle Butte and Gateway Quadrangles, Jefferson and Wasco Counties, Oregon: Oregon Department of Geology and Mineral Industries Geologic Map Series GMS-43, scale 1:24,000, https://www.oregongeology.org/pubs/gms/GMS-044.pdf.

Smith, G.A., Snee, L.W., and Taylor, E.M., 1987, Stratigraphic, sedimentologic, and petrologic record of late Miocene subsidence of the central Oregon High Cascades: Geology, v. 15, p. 389–392, https://doi.org/10.1130/0091-7613(1987)15<389:SSAPRO>2.0.CO;2.

Smith, G.A., Vincent, K.R., and Snee, L.W., 1989, An isostatic model for basin formation in and adjacent to the central Oregon High Cascade Range, *in* Muffler, L.P.J., Weaver, C., and Blackwell, D., eds., Geological, Geophysical, and Tectonic Setting of the Cascade Range: U.S. Geological Survey Open-File Report 89-178, p. 411–428, https://doi.org/10.3133/ofr89178.

Stearns, H.T., 1931, Geology and water resources of the middle Deschutes River basin, Oregon: Chapter D, *in* Contributions to the Hydrology of the United States, 1930: U.S. Geological Survey Water-Supply Paper 637, p. 125–212, https://doi.org/10.3133/wsp637.

Steiger, R.H., and Jäger, E., 1977, Subcommission on Geochronology: Convention on the use of decay constants in geo- and cosmochronology: Earth and Planetary Science Letters, v. 36, no. 3, p. 359–362, https://doi.org/10.1016/0012-821X(77)90060-7.

Swanson, D.A., Anderson, J.L., Camp, V.E., Hooper, P.R., Taubeneck, W.H., and Wright, T.L., 1981, Reconnaissance Geologic Map of the Columbia River Basalt Group, Northern Oregon and Western Idaho: U.S. Geological Survey Open-File Report 81-797, sheet 1, scale 1:250,000, https://doi.org/10.3133/ofr81797.

Tauxe, L., 2010, Essentials of Paleomagnetism: Berkeley, California, University of California Press, 489 p., https://doi.org/10.1525/9780520946378.

Thorarinsson, S., 1968, On the rate of lava- and tephra production and the upward migration of magma in four Icelandic eruptions: Geologische Rundschau, v. 57, no. 3, p. 705–718, https://doi.org/10.1007/BF01845358.

U.S. Geological Survey, 2022a, USGS 1/3 Arc Second n45w122 20220426: U.S. Geological Survey, https://data.usgs.gov/datacatalog/data/USGS:3a81321b-c153-416f-98b7-cc8e5f0e17c3 (accessed 26 April 2022).

U.S. Geological Survey, 2022b, USGS 1/3 Arc Second n46w121 20221128: U.S. Geological Survey, https://data.usgs.gov/datacatalog/data/USGS:3a81321b-c153-416f-98b7-cc8e5f0e17c3 (accessed 28 November 2022).

Walker, G.P.L., 1973, Lengths of lava flows: Philosophical Transactions of the Royal Society of London A—Mathematical and Physical Sciences, v. 274, p. 107–118, https://www.jstor.org/stable/74335.

Waters, A.C., 1968, Reconnaissance Geologic Map of the Dufur Quadrangle, Hood River, Sherman, and Wasco Counties, Oregon: U.S. Geological Survey Miscellaneous Geologic Investigations Map I-556, scale 1:125,000, https://doi.org/10.3133/i556.

Watson, G.S., 1956, A test for randomness of directions: Geophysical Supplements to the Monthly Notices of the Royal Astronomical Society, v. 7, no. 4, p. 160–161, https://doi.org/10.1111/j.1365-246X.1956.tb05561.x.

Wells, R.E., and McCaffrey, R., 2013, Steady rotation of the Cascade arc: Geology, v. 41, p. 1027–1030, https://doi.org/10.1130/G34514.1.

Wells, R.E., Weaver, C.S., and Blakely, R.J., 1998, Forearc migration in Cascadia and its neotectonic significance: Geology, v. 26, p. 759–762, https://doi.org/10.1130/0091-7613(1998)026<0759:FAMICA>2.3.CO;2.

Windom, K.E., Stewart, D.C., and Thornton, C.P., 1981, Development of columnar-spheroidal structures by meteoric water in a New Mexico basalt: Geology, v. 9, p. 73–76, https://doi.org/10.1130/0091-7613(1981)9<73:DOCSBM>2.0.CO;2.

Woodring, D.N., 2020, Kinematics of the Columbia Hills Anticline and the Warwick Strike-Slip Fault, Yakima Fold and Thrust Belt, Washington, USA [M.S. thesis]: Corvallis, Oregon, Oregon State University, 108 p.

Yuh, I.P., Evarts, R.C., and Conrey, R.M., 2022, X-ray Fluorescence Geochemistry of Columbia River Basalt Group Rocks in the Western Columbia River Gorge: U.S. Geological Survey Data Release, https://doi.org/10.5066/P9Z2XK4E.

Zijderveld, J.D.A., 1967, AC demagnetization of rocks—Analysis of results, *in* Collinson, D.W., Creer, K.M., and Runcorn, S.K., eds., Methods in Paleomagnetism: Amsterdam, Elsevier, p. 254–286.

Science Editor: Brad Singer
Associate Editor: Richard Waitt

Manuscript Received 9 June 2023
Revised Manuscript Received 19 October 2023
Manuscript Accepted 6 December 2023